Available on CMS information server **CMS NOTE 1997/043**

The Compact Muon Solenoid Experiment

CMS Note

Mailing address: CMS CERN, CH-1211 GENEVA 23, Switzerland

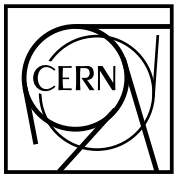

May 30, 1997

External and final state internal bremsstrahlung effects and Higgs mass reconstruction in $H \rightarrow ZZ^* \rightarrow 4e^{\pm}$ for M_H=130GeV

C. Charlot

LPNHE-Ecole Polytechnique, IN2P3-CNRS, Palaiseau, France

I. Puljak

University of Split, Split, Croatia

Abstract

The effect of external as well as internal bremsstrahlung radiation in $H \rightarrow ZZ^* \rightarrow 4e^{\pm}$ channel is studied in full detector simulation. A method is proposed for external and internal bremsstrahlung recovery, allowing us to use $\geq$ 95% of electrons within $\mid E/p_{gen} - 1 \mid \leq 0.2$. It is shown that traditional E/p and isolation cuts can be implemented with $\geq$ 90% efficiency, but that precise mass reconstruction is achievable with higher efficiency without applying such cuts. Z and Higgs reconstruction efficiencies are given, in presence of jet background from the underlying event. The final efficiency for Higgs reconstruction within $\pm 2\sigma$ amounts to 37%, with a resolution of 0.85 GeV for a realistic PbWO4 calorimeter. The resolution drops to 1.28 GeV for a pessimistic version of the calorimeter resolution.

1 Introduction

The search for the Standard Model Higgs boson in the intermediate mass range 120 GeV $\leq M_H \leq$ 180 GeV relies on the H $\rightarrow \gamma\gamma$ and on the H $\rightarrow$ ZZ* $\rightarrow$ 4l$^{\pm}$ channels. For the latter, lepton momentum down to low p_t values (p_t $\geq$ 5 GeV) is desirable and a rapidity coverage up to $\eta \leq 2.5$ is needed to detect efficiently the four leptons [1]. Excellent precision has to be achieved because the Higgs is very narrow in this mass range (width below 10 MeV at 130 GeV) and therefore the signal significance is governed by the instrumental resolution. Excellent reconstruction efficiency per lepton is also particularly needed in this channel due to the necessity of detecting four leptons.

For the four electrons decay mode, excellent precision is in principle achievable with the CMS inner tracker and the PbWO4 crystal ECAL. However, it has already been stressed that external bremsstrahlung radiation in the tracker material may limit significantly the possibility of electron momentum measurement by the tracker. It has been shown that this loss can be partly recovered using the calorimeter information [2, 3].

In addition, internal bremsstrahlung, i.e. the emission of a photon in the Z decay, changes the four momentum reconstruction and leads also to a loss of signal reconstruction efficiency and degradation of mass resolution [1].

These questions have been already investigated in previous studies [2, 3]. We present here updated results with more emphasis on external radiation and its correlation with tracks reconstruction. We also investigate the question of electron identification in this channel. The proximity of photon clusters around electrons, either from internal or external bremsstrahlung may affect the efficiency of electron identification, in addition to the need of accurate estimate of the electron and photon energies. Finally, to obtain realistic estimates of the reconstruction efficiencies, electron identification is studied with full event simulation including hadronic background from the underlying event.

The study has been done for the nearly lower Higgs mass reachable in this channel (130 GeV), resulting in a lower electron p_t and hence most problematic detection. Quantitative results for reconstruction precision and efficiencies for Z and H are given for optimistic, pessimistic and realistic parametrisation of the ECAL resolution defined in the following.

2 Simulation tools

The presented study has been made using the GEANT3.21 based simulation package CMSIM/CMANA version 8 [4]. The Higgs signal has been generated using PYTHIA5.7, with standard p_t cuts of 10, 10, 15 and 20 GeV on the four electrons. A dedicated package, PHOTOS [5], has been used to account for internal radiation in Z decays. Events were passed through CMSIM for the GEANT detector simulation, with a cutoff of 10 MeV for the photon radiation. The geometry used (ICVERS=10) corresponds to the TP design [6]. For the tracker, it consists in an average geometry built on concentric cylinders and forward disks (ITVERS=2). The tracker cables and services are not included in the simulation. For the ECAL, we use the external geometry (IEVERS=-120) in which each crystal has a square size $20.5 * 20.5$ mm^2. Tilt of the crystal axis is not included. The preshower was not included in the present simulation. To simulate electromagnetic showers, we use the semi-fast version of the electromagnetic calorimeter description in which longitudinal and transverse shower profiles and their fluctuations are parametrized and where the fluctuations of energy response according to

$$\frac{\sigma_E}{E} = \frac{0.035}{\sqrt{E}} \oplus 0.007$$

are introduced [7]. Optimistic

$$\frac{\sigma_E}{E} = \frac{0.02}{\sqrt{E}} \oplus 0.005$$

and pessimistic

$$\frac{\sigma_E}{E} = \frac{0.05}{\sqrt{E}} \oplus 0.01$$

assumptions on the final calorimeter resolution are also simulated.

The simulated data are then passed through CMANA for electronic noise addition, and then undergo final reconstruction and analysis. A gaussian uncorrelated electronic noise of σ=25 MeV (50 MeV in the pessimistic version of the ECAL resolution) is introduced. A digitisation is introduced with a quantization error of 25 MeV. A threshold corresponding to 1σ of the noise is applied on simulated data. Finally, a selected readout intended to reduce the data volume is applied: only the energy in a window of $3 * 3$ trigger cells ($18 * 18$ crystals) around direction of each particle with $p_t \geq 5$ GeV is recorded.

Track fitting is performed using CMSIM 8 implementation of a Kalman-Filter algorithm. A minimum (maximum) of 4 (25) track clusters is required to build a track, with a maximum gap of 30 cm between two consecutive track clusters. Track finding is not included.

The clusterization algorithm of [8] is used to reconstruct electrons and photons in the ECAL. A self-correction for loss due to digitisation and zero skipping is applied, as illustrated on Fig. 1.

The CMSIM/CMANA data model is used to retrieve the crystals from electromagnetic clusters and the Monte Carlo incoming particle(s) and the reconstructed track(s) related to each cluster. This is particularly useful in analysing track/cluster matching in presence of overlapping showers.

3 External bremsstrahlung radiation

The emission point of external bremsstrahlung photons for electrons from a Higgs decay (mean p_t about 31.4 GeV) and limited to $\eta \leq 1.6$ is shown in Fig. 2. The amount of tracker material in terms of radiation lenght before the ECAL is 0.25X_0 at η=0, increasing to 0.6X_0 at η=1.6 [6]. In view of the current tracker mechanical design, this should be considered as a very optimistic assumption on the final tracker material budget. In particular, the tracker cables and services are not accounted for. The layer at R = 140 cm corresponds to a realistic description of the material before the crystal entry face: the structure consists of two skins of 4mm thick carbon filled by 20 mm polyethylene as a neutron moderator. This set is 2mm before the crystal entry face and amount to 0.084X_0 at η=0. One should notice the important contribution from the beam pipe and the two pixels layers, which lead to photon emission at the very begining of the electron track (R_t=6, 7, and 12 cm respectively). The p_t spectrum of emitted photons is also shown in Fig. 2.

The external bremsstrahlung is more important at high η and for low p_t due to the increased track lenght and curvature in the strong CMS magnetic field. The track p, η, ϕ resolutions from the Kalman-Filter track fit for electrons from a Higgs decay are shown in Fig. 3. The low energy tail in the momentum distribution is due to bremsstrahlung emission. The degradation in momentum resolution can be seen in Fig. 4 which shows the track Δp distribution as a function of the number of emitted photons.

The correlation between the quality of track reconstruction and the bremsstrahlung emission point is shown in Fig. 5. From this, one can distinguish three regions in the transverse radius of emission:

i) R$\leq$15cm, where the track parameters are modified at the very begining. Unless the pixel detectors are able to perform self correction, a correct mass reconstruction can only be achieved with the help of the ECAL information. From the ECAL point of view, emitted gammas give clusters well separated from the electron cluster most of the time. They look like internal bremsstrahlung (see next section).

ii) 15cm$\leq$R$\leq$80cm: here, the track fit gets worse, with a maximum loss at R $\sim$ 80cm corresponding to a kink at about the middle of the track lenght. The ECAL could help, but gammas are separated from the electron cluster for very low p_t electrons, or if the gamma takes an important fraction of the electron momentum.

iii) R$\geq$80cm, where the modification of track parameters is marginal. The emitted photons are undistinguishable from the electron cluster. Such photons do not generate significant efficiency losses. There is, however, still a probable loss in ECAL precision, due to preshowering of the electron.

It is clear that for low p_t electrons, one should correlate the ECAL and TRAK information to optimize reconstruction. A track refit using additionnal ECAL information that can be introduced in the Kalman-Filter method could be implemented. However, it appears from the above discussion that the most important part of the effect, when photons are emitted at the very beginning, can be corrected for by applying an external bremsstrahlung recovery procedure using ECAL information only ([8]).

Following the procedure described in [8], the photons bremsstrahlung clusters are searched in a phi road starting from the electron cluster, and up to a maximum $\Delta\phi_{max}$ calculated from the electron measured E_t. This is illustrated in Fig. 6 which shows the clusters recovered around electrons. The road is clearly visible within $\pm$ one crystal extension in η, and up to about 0.1 in ϕ (corresponding to the lowest electron E_t considered). For positrons, the recovered clusters are at positive $\Delta\phi$, so that $\Delta\phi_{max}$ is also a function of the charge q. Some bremsstrahlung energy is also recovered outside this road, within $\Delta R \leq 0.05$ around the electron cluster. This is related to internal radiation and will be discussed in the next section.

The effect of the external bremsstrahlung recovery is well illustrated by the change of the distribution of E over p where E is the measured ECAL energy respectively without and with recovery, and where p is the *generated* electron momentum (Fig. 7). The fraction of electron clusters with E/p_{gen} between 0.8 and 1.2 increases from

86.8% (no recovery) to 97.6% (with recovery). It is usefull to compare these distributions with the ones of Fig. 8, where p is here the *reconstructed* track momentum. Since well separated gamma clusters mostly originate from inner radii, the track parameters are determined after bremsstrahlung emission and hence match better the E distribution without recovery. This emphasises the need of an algorithm able to separate as much as possible bremsstrahlung gamma clusters from the electron energy flow.

4 Internal bremsstrahlung radiation

As pointed out in previous sudies [3, 6], the internal radiation from Z $\rightarrow$ e^+e^- decay is potentially also an important source of electron losses. Contrary to external bremsstralung, this loss can only be recovered using the ECAL.

This question has been investigated using a dedicated package, PHOTOS, for the simulation of final state QED radiation in the Z decay.

The potential problem is illustrated in Fig. 9 showing the Z mass distribution at generation level for events with internal bremsstrahlung, with and without including the internal bremsstrahlung photon in the mass calculation. The rate is found to be approximately one internal bremsstrahlung per Higgs event, with a momentum distribution much harder than for external emission, as shown in Fig. 10. The mean photon E_t is about 4.4 GeV.

Also shown in Fig. 10 is the angular distance ΔR between the gamma and the associated lepton ($\Delta R = (\eta_e - \eta_\gamma)^2 + (\phi_e - \phi_\gamma)^2)^{\frac{1}{2}}$) , and the integral of this distribution. One can see that in about 25% of the cases, internal bremsstrahlung is produced in the original electron direction, and hence will be recovered at $\Delta\phi_{max}$ using the recovery procedure designed for external bremsstrahlung. In order to cope to some extent with the photons at ΔR significantly different from 0, it is proposed for internal bremsstrahlung recovery to search for photons in a cone around $\Delta\phi_{max}$ of size ΔR=0.05. It can be seen from Fig. 10 that going to higher ΔR would bring only marginal gain, while increasing potential π^0 contamination and presumably also inducing more electronic noise since more crystals are involved. As for external bremsstrahlung, the photon energy is added to the nearby electron, whose reconstructed track direction will be used for the Higgs mass reconstruction. The photons emitted with larger ΔR could be searched as additionnal isolated photons. However, it is likely that they will be lost in the widst of the π^0 background. The Z invariant mass could be used to identify these extra photons, but it would concern only the on-shell Z.

To summarize, the final recovery algorithm searches bremsstrahlung photons both external and internal ones, around the electron position (η_{rec}, ϕ_{rec}) in a ϕ road up to $\phi_{rec} + \Delta\phi_{max}(E_t, q)$ and in a cone of size ΔR=0.05 around $(\eta_{rec}, \phi_{rec} + \Delta\phi_{max})$.

The E/p_{gen} distribution for Higgs electrons, including internal bremsstrahlung, is shown on Fig. 11 with and without external plus internal bremsstrahlung recovery. As compared to Fig. 7, clusters appear to have more often $E/p_{gen} \geq 1$ due to the inclusion of additionnal photons from internal radiation. The fraction of electron clusters with E/p_{gen} between 0.8 and 1.2 increases from 83.0% (no recovery) to 95.5% (with recovery).

5 Electron identification and Higgs reconstruction

In a realistic event, electrons from the Higgs will be produced on top of possible recoil jets coming from the pp collision and the underlying event. At high luminosity, these are the additionnal pp collisions in the same bunch crossing, an average 17 of them at an instantaneous luminosity of 10^{34}cm^{-2}s^{-1} It is interesting to see how the recovery procedure may be affected by π^0 contamination in such a full event. In addition, this background is used to optimize electron identification cuts in order to provide realistic estimate of Higgs mass reconstruction efficiency and precision. The search for electrons proceeds through the following steps:

- reconstruct all ECAL clusters
- search geometricaly matching reconstructed tracks and ECAL clusters
- select tracks coming from interaction vertex
- select isolated track/cluster associations
- select $\frac{E}{p}$ matched track/cluster associations

The geometrical matching of a cluster with a track is done using helix extrapolation of the track parameters. Both track and ECAL cluster (E $\geq$ 2 GeV) positions have been extrapolated to crystal entry face, to be insensitive to the shower length (this is strictly speaking only true for non tilted geometry). The ECAL cluster position has been estimated using simple barycenter, without S-shape correction. As a consequence the distance between track extrapolation and cluster has precision limited to about 4mm, as shown on Fig. 12. The closest track within $\Delta R \leq$ 0.1 which satisfy $E/p \geq 0.25$ is associated to the cluster. The efficiency of such geometrical matching for electrons is 97.5%.

The distribution of the track/cluster distance for other than Higgs electron tracks coming from the underlying event, and for cluster energy greater than 2 GeV, is also shown on Fig. 12. Electrons candidates are selected if distance is less than 2.2 cm. The efficiency of this cut is 97.5%.

To select primary electrons, it is also asked that the track has one cluster in the first pixel layer ($R_t^{beg} \leq$ 8cm). The acceptance of this cut for Higgs electrons is 98.7%. This cut removes electrons from photon conversions (except for conversions in the beam pipe), as can be seen in Table 1.

No track χ^2 cut has been applied, in order not to loose too much in efficiency (see Fig. 13).

At the generation level, a p_t cut of 10 GeV has been applied on the softer electrons: this threshold has been determined in earlier studies [1] on signal detectability in presence of physics backgrounds. However, reconstructed electrons may have transverse energy below this cut due to external bremsstrahlung. Removing clusters with $E_t \leq$ 10 GeV leads to an 8% loss on reconstructed softer electrons (and hence an 8% loss on Higgs). One may use the external recovery procedure at the reconstruction level to recover these events. To avoid increasing the hadronic background, it is preferable to use $E_t^{recovered} = E_t * E^{recovered}/E$ with E_t from ECAL cluster than $P_t^{recovered} = P_t * E^{recovered}/E$ with p_t from charged tracks. The efficiency of $E_t^{recovered} \geq$ 10 GeV (for p_t at generation greater than 10 GeV) is 93.9% per electrons. It is interesting to look in more details at this bremsstrahlung recovery efficiency at p_t=10 GeV. If one selects only track/cluster associations where the cluster is effectively initiated by an electron, the efficiency is 99.1%, that is less than 1% loss. But in about 3.5% of the electron associations, it happens that the electron track is matched with the photon cluster instead of the electron cluster due to a very hard bremsstrahlung emission ($E_\gamma \geq E_{e^-}$). In this case the recovery fails since the road is defined in the wrong direction due to wrong charge assignment.

A first sample is obtained with the above selection. It is labeled "loose sample". The number of track-cluster associations surviving the above cuts is summarised in Table 1. The efficiency per electrons is 90.1% and purity is 99.3%.

In order to improve electron identification and mass resolution, we further study isolation and E/p matching cuts.

The isolation parameter is defined as ratio of the p_t of the electron candidate, to the summed p_t of all reconstructed tracks within a cone of ΔR=0.1 around the electron candidate. The distribution of this isolation parameter is shown in Fig. 14, for Higgs electrons and other than Higgs electron track-cluster associations which pass the vertex origin criteria and have $E \geq$2 GeV. Higgs electron candidates are selected requiring the isolation parameter to be $\geq$ 0.8. The acceptance of this cut for Higgs electrons is 98.5% per electron with a $\pi^\pm$,K$^\pm$ rejection of $\sim$ 10.

The energy matching between electron candidate track and cluster has to be used with care in presence of bremsstrahlung. It is however the only way to reject isolated a possible contamination by charged pions. Fig. 15 shows the $\frac{E}{p}$ distribution for electrons including external and internal radiation, where E is the cluster energy without recovery and p the reconstructed momentum. It seems that best E/p is obtained *without recovery*. This is due to the fact that recovered clusters are mainly photons emitted at the very begining resulting in a track that does not match in energy the electron cluster. A cut at $\mid E/p - 1 \mid \leq 0.2$ has an efficiency of 91.0% per electron.

Electrons of the "loose sample" passing these isolation and E/p matching cuts are labbeled "restricted sample". The details on cut acceptances and background rejection can be seen in Table 1. The efficiency for the "restricted sample" is 80.8% with a 99.9% purity.

The distributions of the number of electron candidates for the "loose" and "restricted" sample are given in Table 2.

Once the electron cluster/track associations have been selected, the Higgs decay topology is selected by asking:

- at least 4 cluster/track associations
- the 4 electrons selected have to satisfy charge criteria, that is 2 positive and 2 negative tracks.

If more than 4 electron candidates are selected, we take the four highest p_t tracks satisfying the charge constraints.

No other topological cuts are used since the physical backgrounds are not studied here. They are discussed in [1].

The Higgs mass is then reconstructed as a 4-electron invariant mass, using for the electron momentum the measured energy in the ECAL with bremsstrahlung recovery and using the reconstructed track direction at the vertex production.

The Higgs mass is also reconstructed using a cut on Z mass which can help to reduce the $t\bar{t}$ background ([1]). For this, the Z is searched as the pair of opposite sign electrons with the invariant mass closest to the nominal Z mass. The corresponding mass is required to be within $\pm$ 3 GeV of the nominal value.

6 Full results with underlying event

The reconstructed e^+e^- electron mass is plotted in Fig. 16 for the realistic version of the ECAL resolution and using the "loose selection". PHOTOS internal radiation and the external plus internal bremsstrahlung recovery method are included. Also shown is the Z mass fit. The Z mass resolution is 1.7 GeV.

Fig. 17 shows Higgs mass reconstruction with and without a Z mass cut, for the realistic version of the ECAL resolution and using the "loose selection". The Higgs mass resolution is 0.85 (0.86) GeV without (with) the Z mass cut.

The low energy tail in the mass distributions can be quantified by the fraction of events with M_H within $\pm 2\ \sigma$. This fraction amounts to 63% (71%) without (with) the Z mass cut, as presented in Table 3. The effective r.m.s (one half of the width which contains 68.3% of the distribution) is also given.

Figs. 18-19 present the results for the "restricted" sample. A better mass distribution is obtained with the "restricted" cuts, but as for the Z mass cut, the price to pay in acceptance is very high (especially due to the $\frac{E}{p}$ match).

The results are summarised in Table 3. They show that efficiency is maximized with loose cuts without sizeable effects on resolution. Rather pure sample is obtain without the isolation and E/p matching cuts due to selection of 4 track-cluster associations and the charge constraints. The loss due to any additionnal cuts is important as it goes as ϵ^4_{ele}. Of course, this optimisation is done from the point of vue of the best electron identification and measurement. For the isolation cut, it will have to be reconsidered in a final analysis including physics backgrounds since isolation is also used to suppress such backgrounds.

One can also see that the Z mass cut, even if it reduces the low mass tail in the Higgs mass distribution, gives about a factor 2 loss in signal acceptance. Consequently, other ways of reducing the physical $Zb\bar{b}$ and $t\bar{t}$ backgrounds as isolation and impact parameter should be prefered.

Finally, results with loose cuts are presented for "optimistic" (Fig. 20-21) and "pessimistic" (Fig. 22-23) versions of the ECAL resolution. They are given for the "loose selection" which maximizes the efficiency. As expected, the pessimistic version of the ECAL resolution leads to a big loss in resolution with σ_H=1.28 GeV (σ_H=1.31 GeV) without (with) Z mass cut. The precision obtained with optimistic ECAL (σ_H=0.93 GeV without and σ_H=0.69 GeV with Z mass cut) is about the same as for realistic ECAL. Results are summarised in Table 4. Statistical errors on σ_H are about 10%.

7 Conclusions

The effects of external and internal bremsstrahlung radiation have been investigated in H$\rightarrow$ZZ*$\rightarrow$4e$^{\pm}$ for M_H=130 GeV. Bremsstrahlung affects both the Higgs mass resolution and the electron reconstruction efficiency. With external plus internal bremsstrahlung recovery, the efficiency for electron energy measurement (E/p_{gen} between 0.8 and 1.2) can be kept above 95%. Realistic electron identification cuts have been introduced, based on the rejection of jet background from the underlying event itself. This criteria should ultimately also be optimised in view of rejecting physics backgrounds. The price of a Z mass cut is to reduce the efficiency by about one third and therefore should be avoid as far as possible. To maximise the detection efficiency, only geometrical matching between the track and the cluster as well as track origin at the vertex are required. The efficiency is found to be 58.2% for Higgs reconstruction with 63% of the events within $\pm 2\sigma$, giving on overall 2σ efficiency of 37% for the realistic ECAL. The Higgs mass resolution is 0.9%, 0.9% and 1.3% respectively for optimistic, realistic and pessimistic versions of the calorimeter resolution. The next step would be to include track finding efficiency, together with a more realistic detector geometry. A refined electron track reconstruction including bremsstrahlung search in track finding/fitting could help for the lowest p_t range. Internal bremsstrahlung far from the electron cluster may be searched for using the Z mass constraint, but only for the on-shell Z. The final optimisation for

electron selection and in particular for electron isolation and recovery criteria should also take into account the need to suppress and control the expected physics backgrounds.

8 Acknowledgements

We 'd like to thank Daniel Denegri and Chris Seez for useful discussions and careful reading of this note.

References

[1] **CMS Note 1995/059**, I. Iashvili, R. Kinnunen, A. Nikitenko and D. Denegri, *"Study of the $H \to 4l^{\pm}$ Channel in CMS"*.

[2] **CMS Note 1995/019**, A. Nikitenko, P. Verrecchia and D. Bomestar, *"I.Z $\to e^+e^-$ and $H \to 4e^{\pm}$ Mass reconstruction in PbWO4 Crystal ECAL with GEANT simulation of CMS Detector. II.Electrons of E_t=30 GeV at η=0.1 and 1.3 in CMS Detector: E/p Matching, Calibration, Resolution"* .

[3] **CMS Note 1995/101**, C. Charlot, A. Nikitenko, I. Puljak, I. Soric, *"Comparison of fixed window and clusterization algorithms for Z$\to e^+e^-$ and $H \to 4e^{\pm}$ mass reconstruction in CMS PbWO4 crystal ECAL for Higgs mass 170 and 130 GeV"*.

[4] **CMS Note 1993/063**, C. Charlot, V. Genchev, V. Karimaki, M. Pimia, P. Moissenz, A. Rosowsky, N. Sinanis and G. Wrochna, *"CMSIM-CMANA Simulation Facilities"*.

[5] E. Barberio, B. Van Eijk and Z. Was, Comp. Phys. Commm. 66 (1991) 115.

[6] "The Compact Muon Solenoid", Technical Proposal, CERN/LHCC 94-38, dec. 94.

[7] **CMS Note 1994/312**, C. Charlot, *"Electromagnetic shower parametrization in CMSIM"*.

[8] **CMS Note 1995/074**, P. Busson and C.Charlot, *"A method for electron/photon reconstruction in CMS PbWO4 crystal ECAL"*.

	Higgs electrons	$\pi^{\pm}$,$K^{\pm}$	electrons (other than Higgs)	others
Track matching and E$\geq$2 GeV	3899	495	165	63
Dist$\leq$2.2 cm	3801	365	142	29
R_t^{beg} $\leq$8 cm	3752	313	7	19
$E_t^{rec} \geq 10$ GeV	3604	19	6	1
$T_{isol} \geq 0.8$	3549	2	4	1
$\lvert E/p - 1 \rvert \leq 0.2$	3230	1	2	0

Table 1: Number of track/cluster associations passing the cuts (for 1000 generated Higgs events)

	N=0	**N=1**	**N=2**	**N=3**	**N=4**	**N=5**
Loose cuts	0.0	0.8	6.5	32.5	56.4	3.8
Restricted cuts	0.5	4.5	19.4	37.7	37.8	0.1

Table 2: The distribution of the number(N) of electron candidates after cuts (in %)

	Entries	Normalisation	Mean value	Sigma	2 sigma efficiency	eff. rms
Loose cuts						
Z + Z*	582	95.0	90.9	1.66	0.52	5.14
Higgs	582	81.8	129.6	0.85	0.63	2.10
Higgs with Z mass cut	305	50.5	129.7	0.86	0.71	1.37
Restricted cuts						
Z + Z*	379	67.4	90.9	1.61	0.58	3.85
Higgs	379	62.6	129.7	0.77	0.72	1.47
Higgs with Z mass cut	220	40.1	129.8	0.79	0.72	1.14

Table 3: Fit results of Z and Higgs mass reconstruction for realistic ECAL for 1000 generated events

	Entries	Normalisation	Mean value	Sigma	2 sigma efficiency	eff. rms
Optimistic						
Z + Z*	547	90.4	90.8	1.68	0.55	4.94
Higgs	547	72.7	129.7	0.93	0.63	2.05
Higgs with Z mass cut	303	50.6	129.9	0.69	0.64	1.44
Realistic						
Z + Z*	582	95.0	90.9	1.66	0.52	5.14
Higgs	582	81.8	129.6	0.85	0.63	2.10
Higgs with Z mass cut	305	50.5	129.7	0.86	0.71	1.37
Pessimistic						
Z + Z*	574	79.8	91.2	1.81	0.63	5.44
Higgs	574	56.0	130.0	1.28	0.65	2.86
Higgs with Z mass cut	279	32.2	130.1	1.31	0.71	2.05

Table 4: Fit results of Z and Higgs mass reconstruction for realistic, optimistic and pessimistic ECAL for 1000 generated events

List of Figures

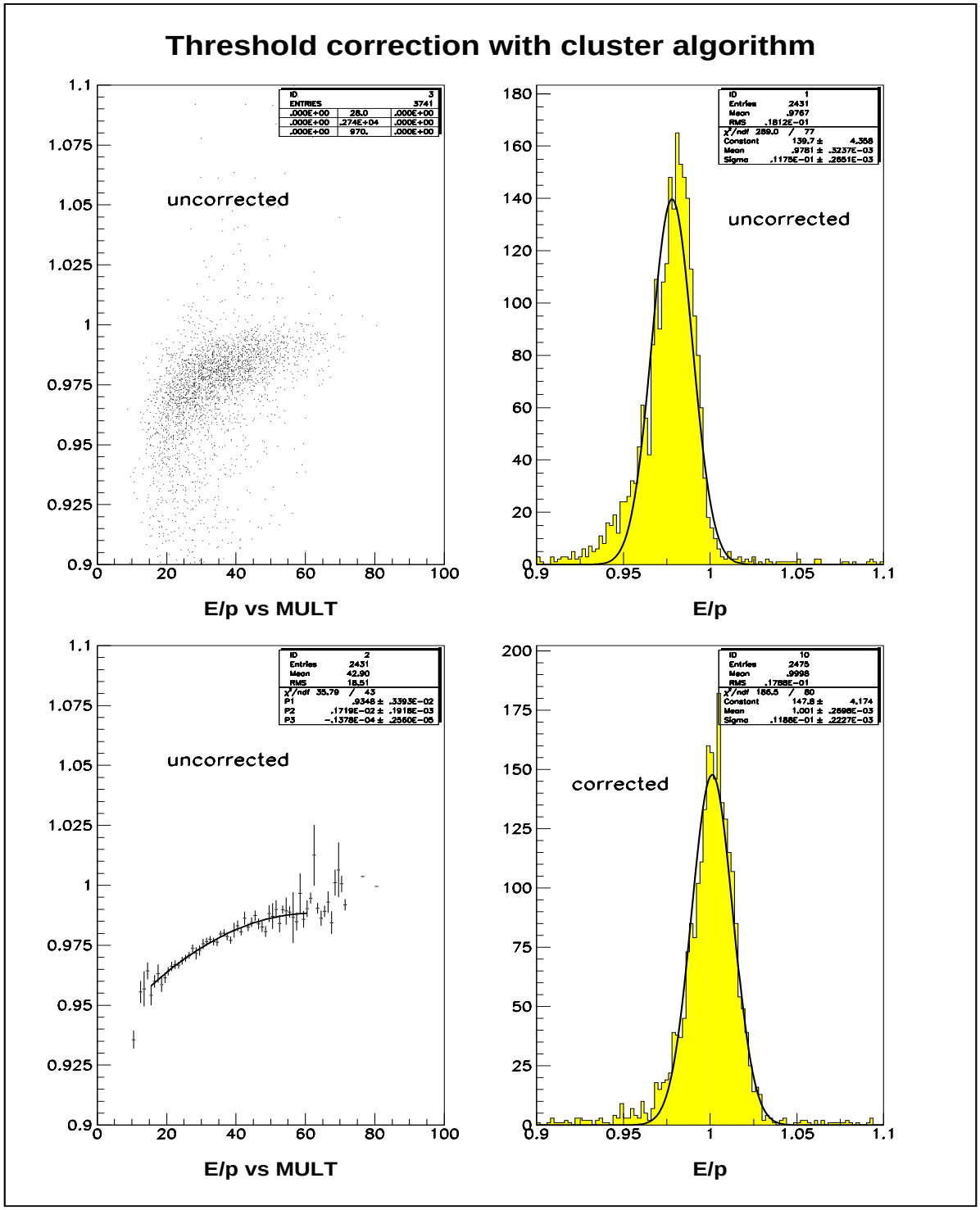

Figure 1: Correction of energy loss due to threshold and digitisation: MULT is the cluster multiplicity.

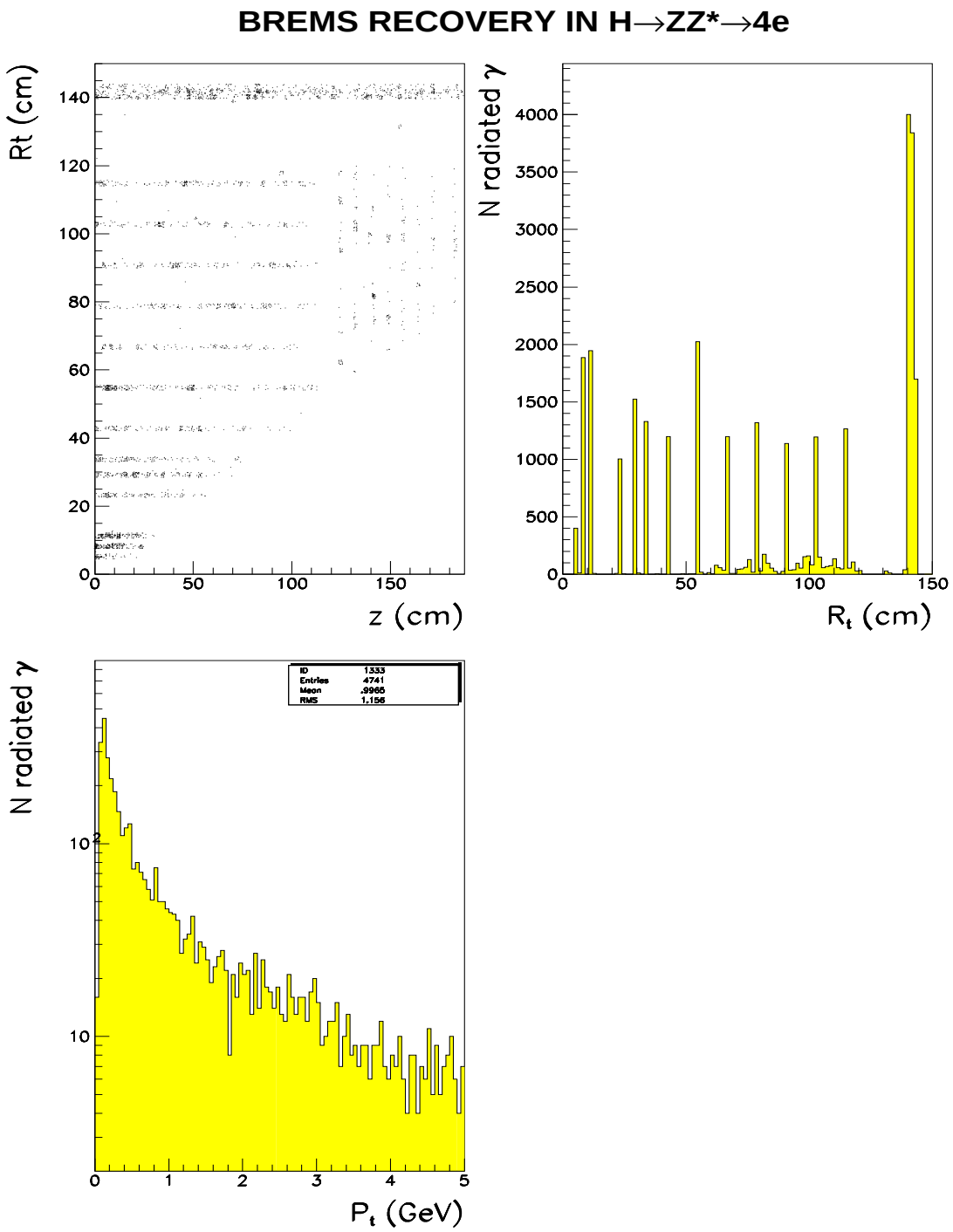

Figure 2: The transversal radius and p_t spectrum of emitted bremsstrahlung for $\eta \leq 1.6$.

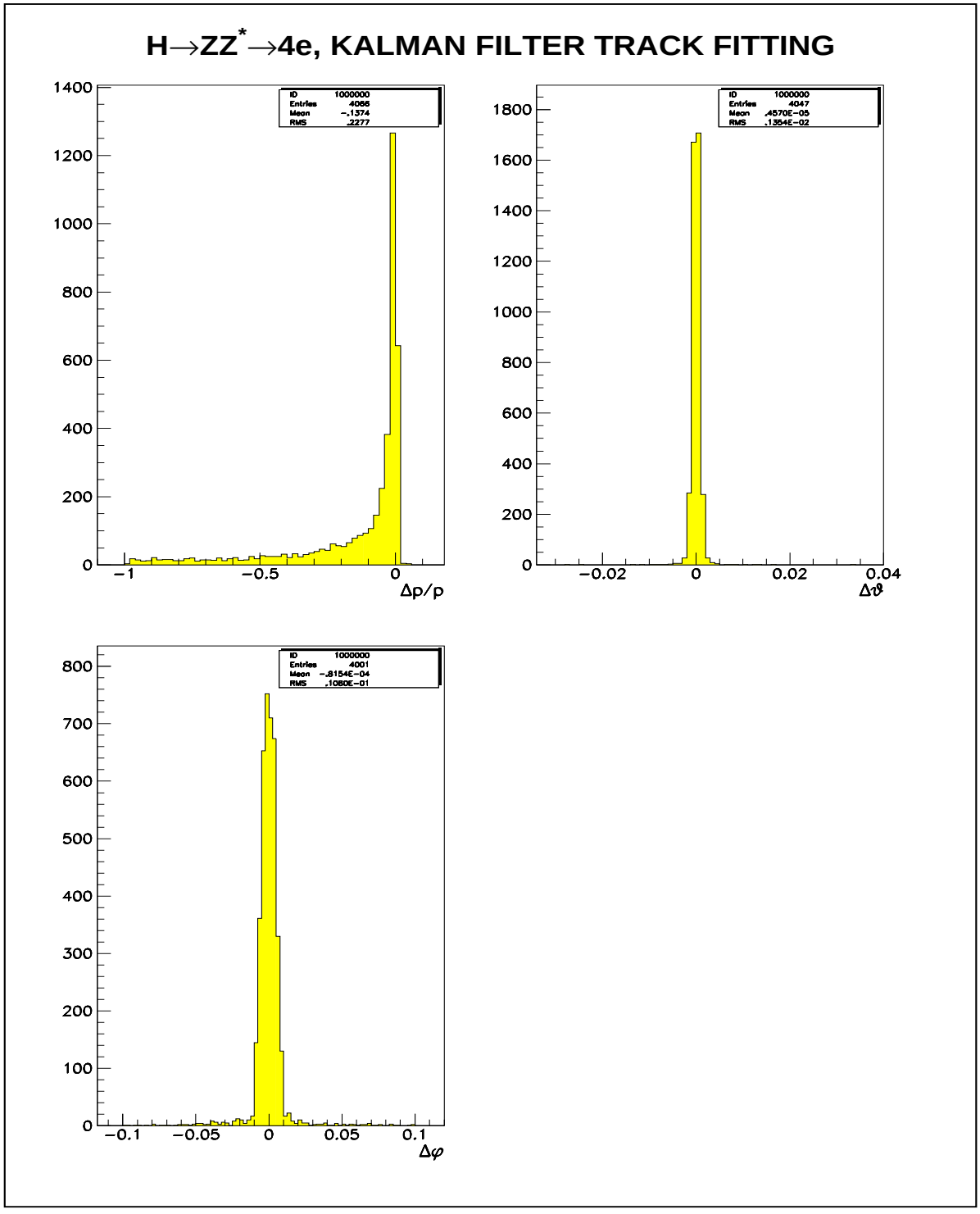

Figure 3: Track fit momentum and angular resolutions for electrons from Higgs decay.

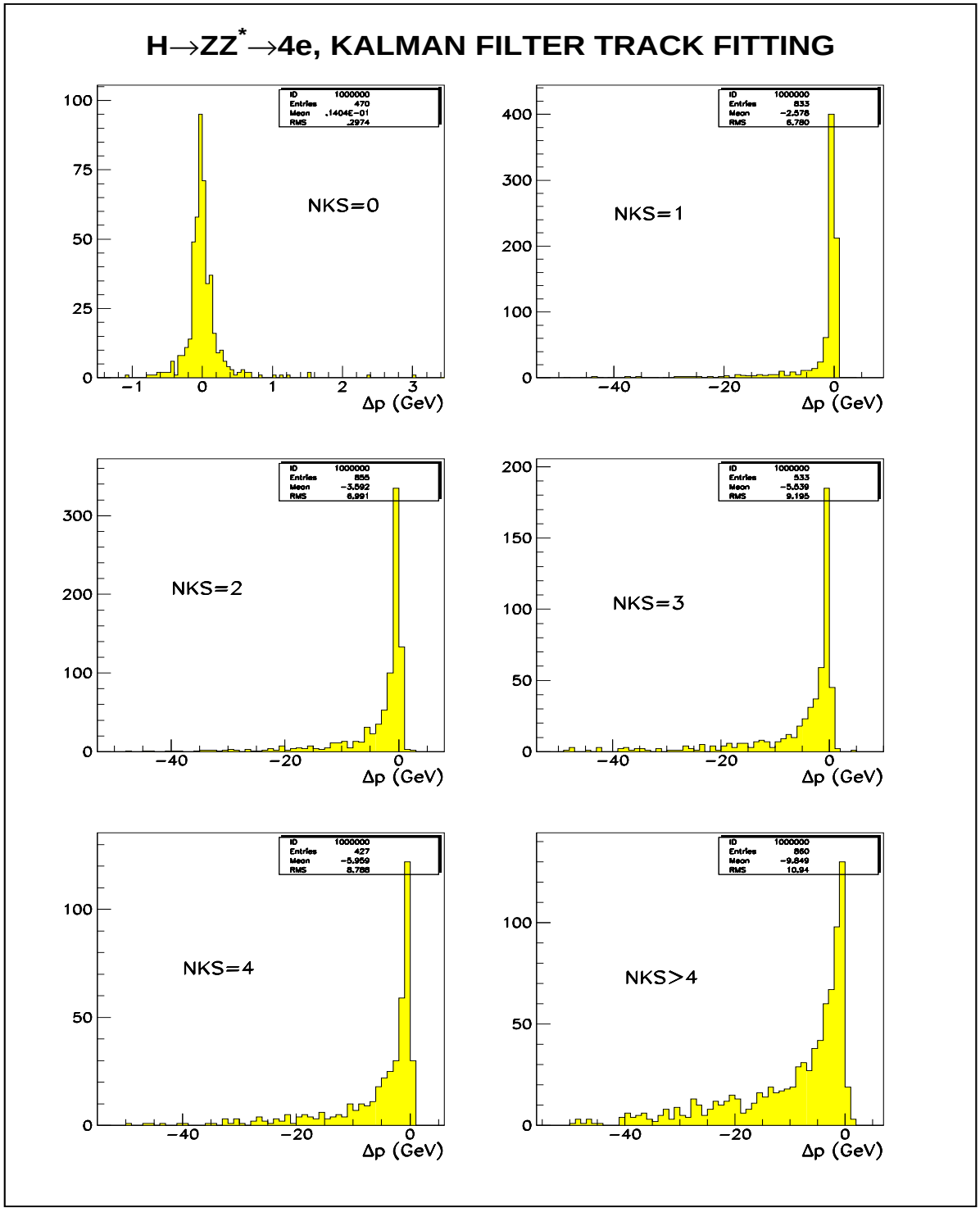

Figure 4: Track Δp as function of the number of emitted secondary gammas (NKS).

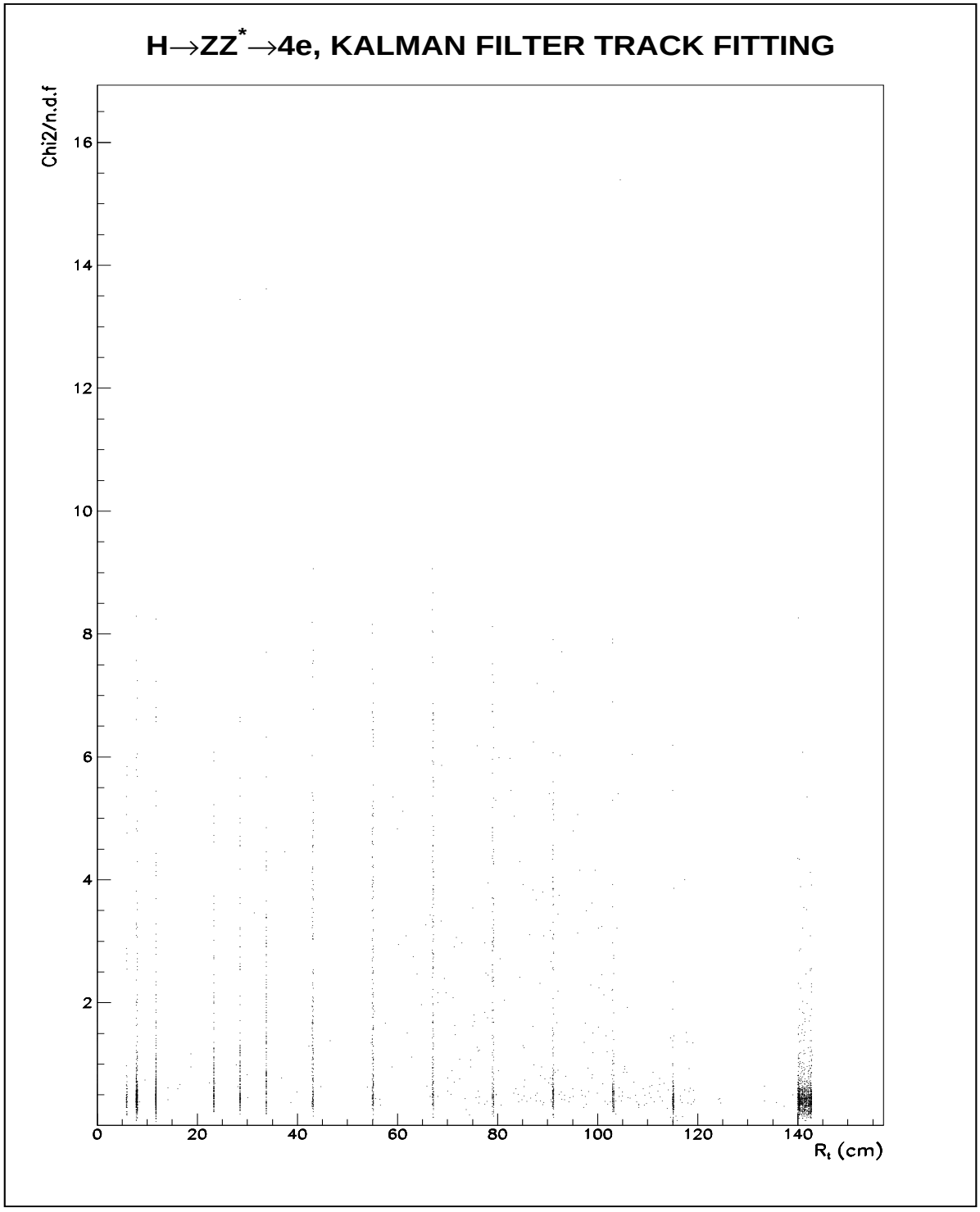

Figure 5: Track χ^2/ndf as function of transverse radius of emitted secondary gammas.

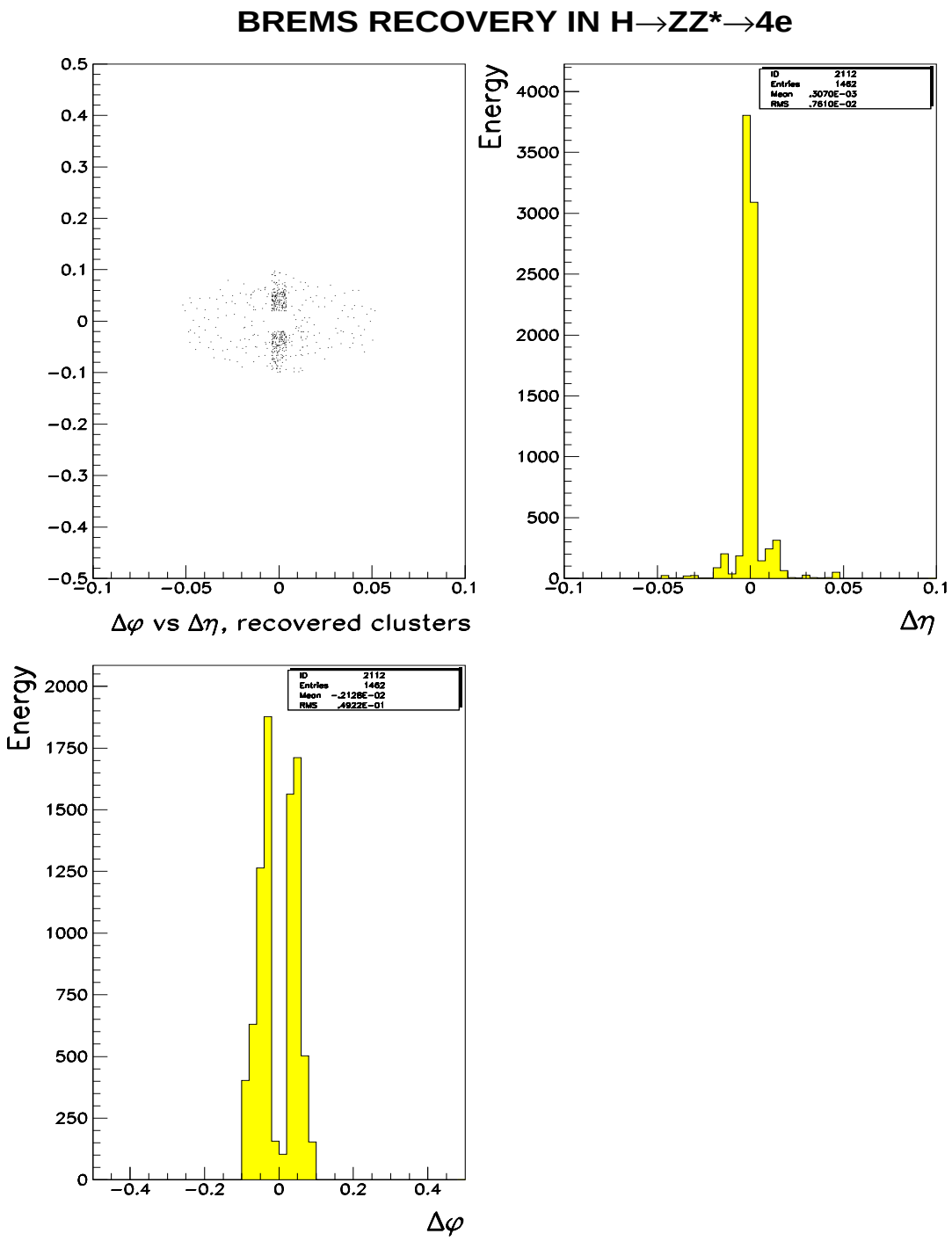

Figure 6: Recovered bremsstrahlung clusters around electron clusters.

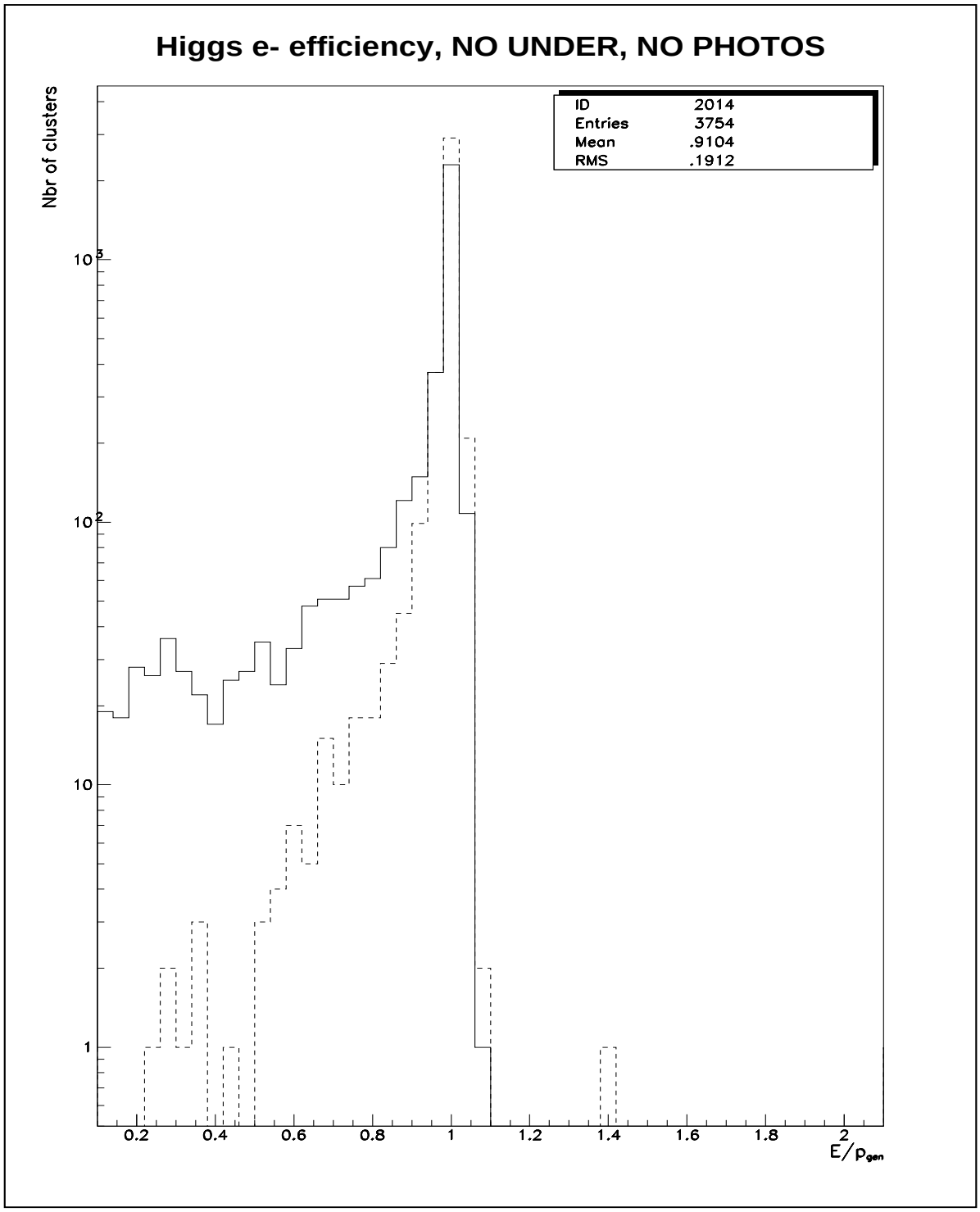

Figure 7: E over p distribution for Higgs electrons with external radiation. E is the ECAL energy without (solid line) and with (dashed line) bremsstrahlung recovery, p the generated electron momentum.

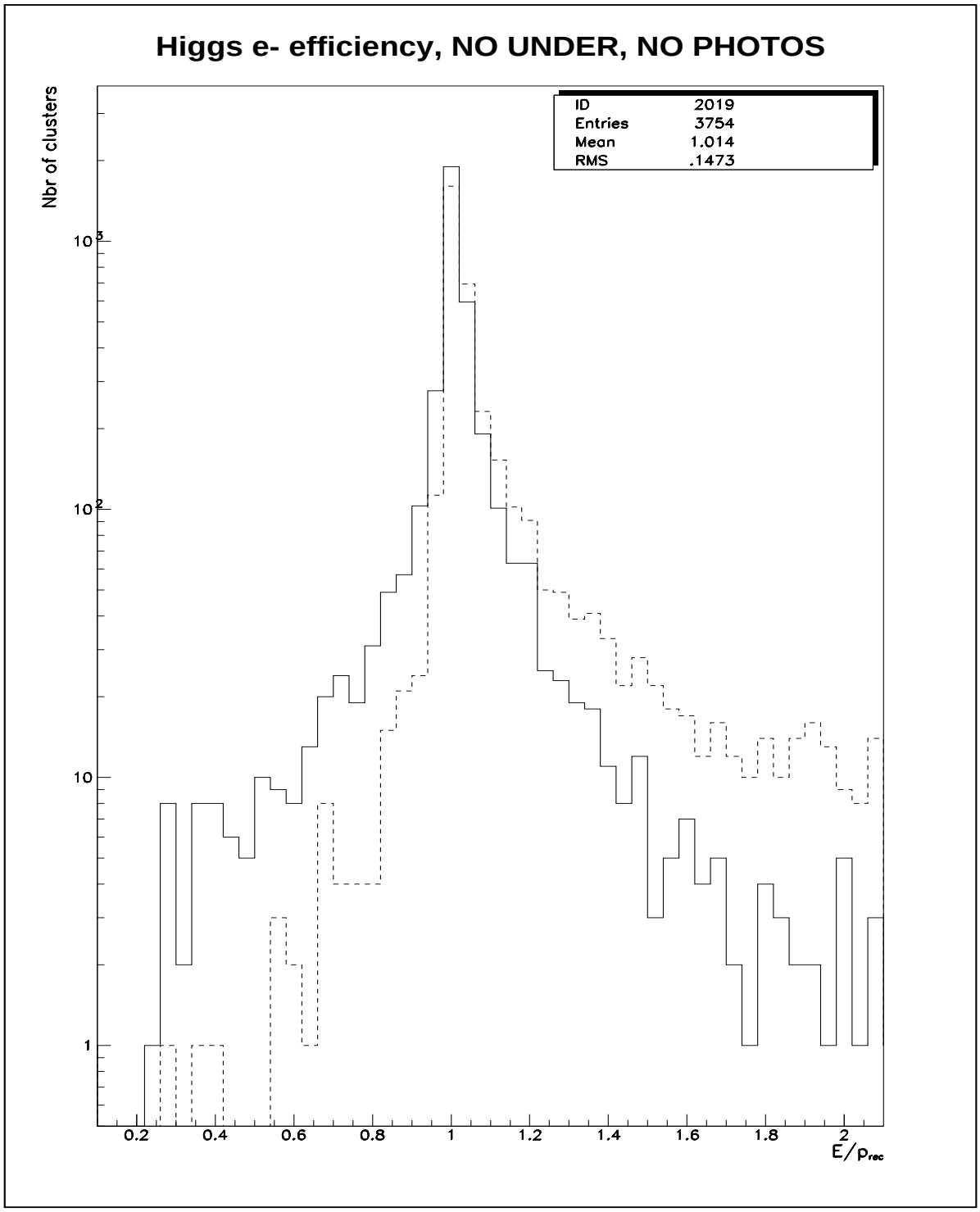

Figure 8: E over p distribution for Higgs electrons with external radiation. E is the ECAL energy without (solid line) and with (dashed line) bremsstrahlung recovery, p the reconstructed track momentum.

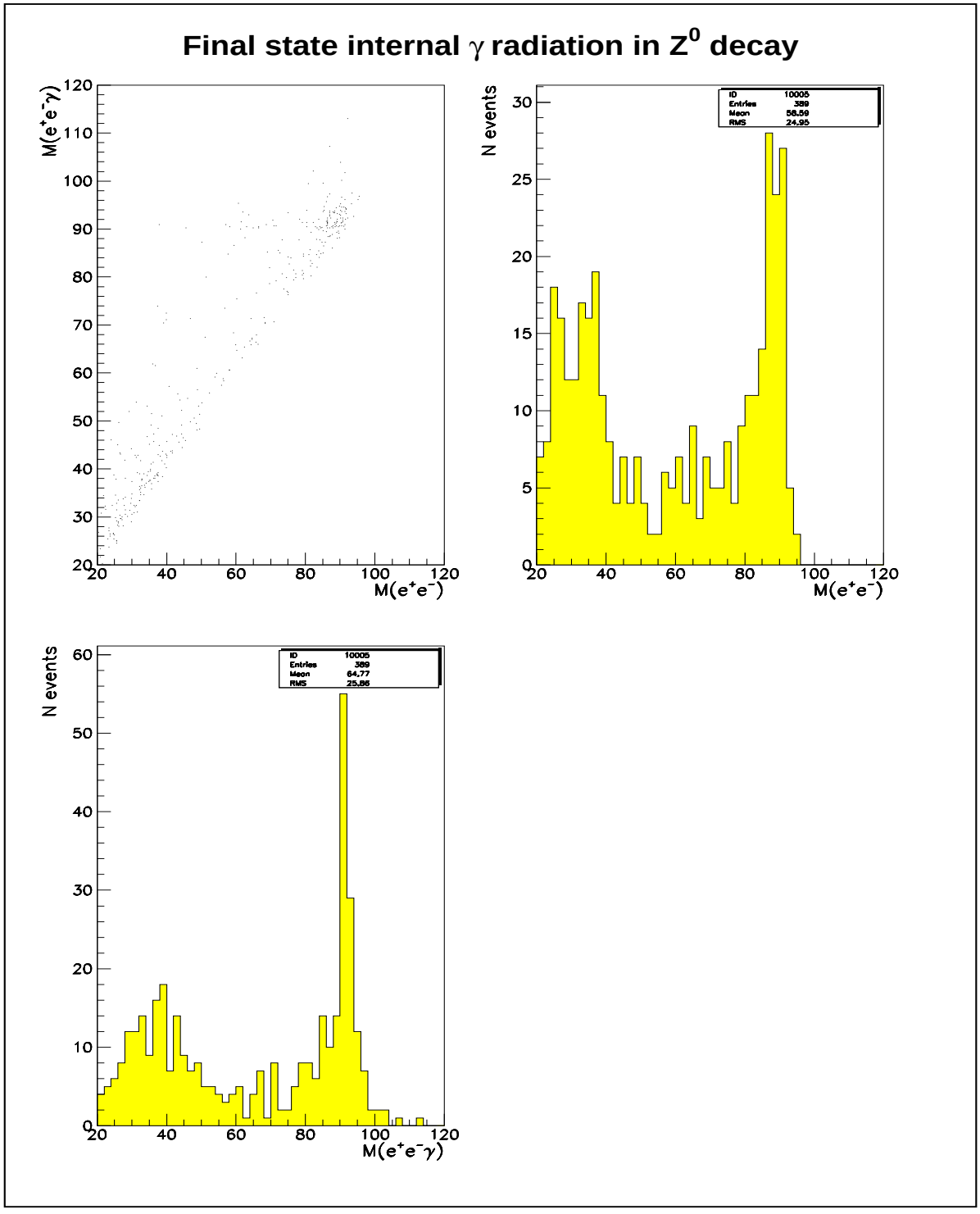

Figure 9: Z mass reconstruction at parton level with and without including internal gamma.

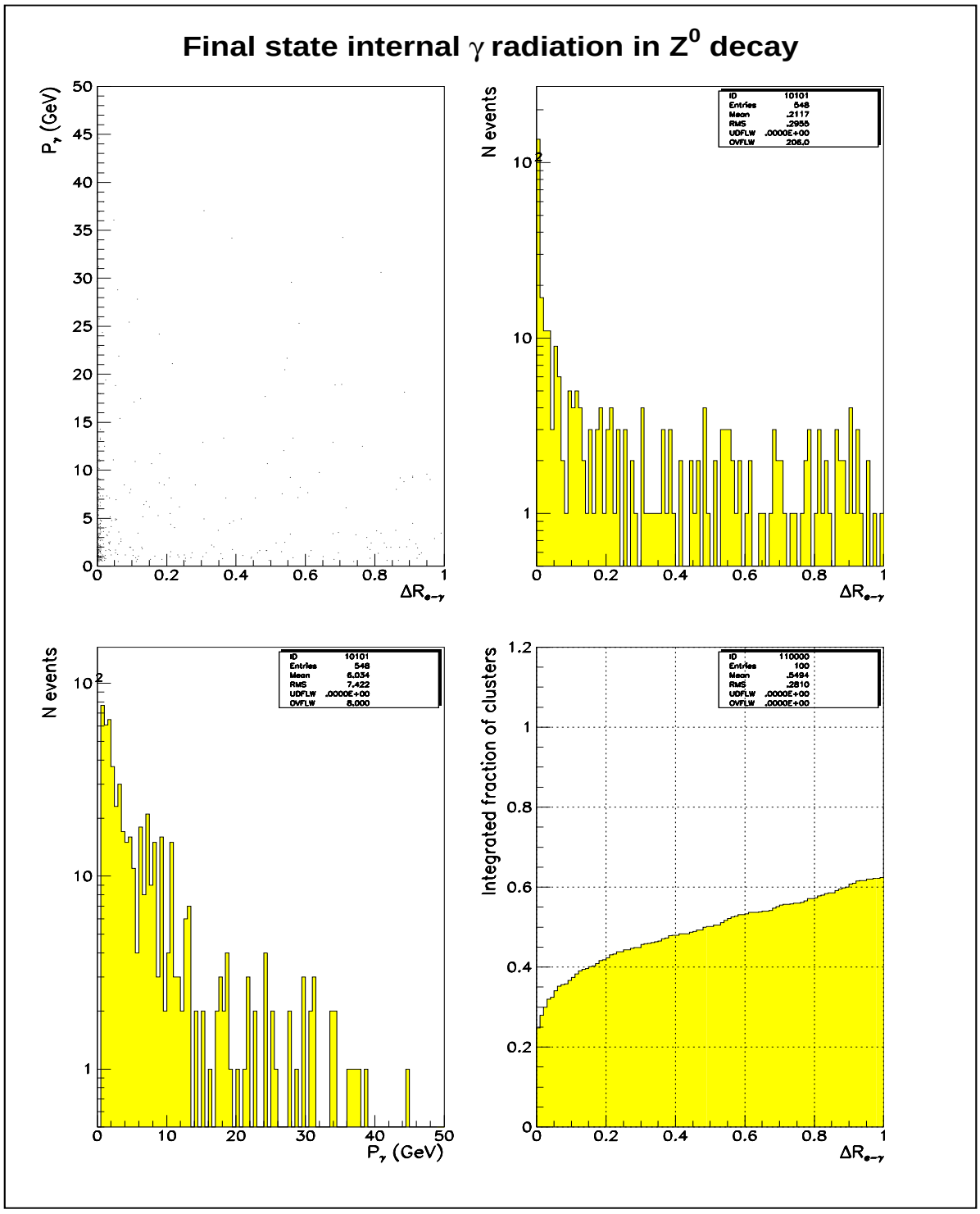

Figure 10: Internal bremsstrahlung momentum distribution vs angular distance to the electron, as given by PHOTOS.

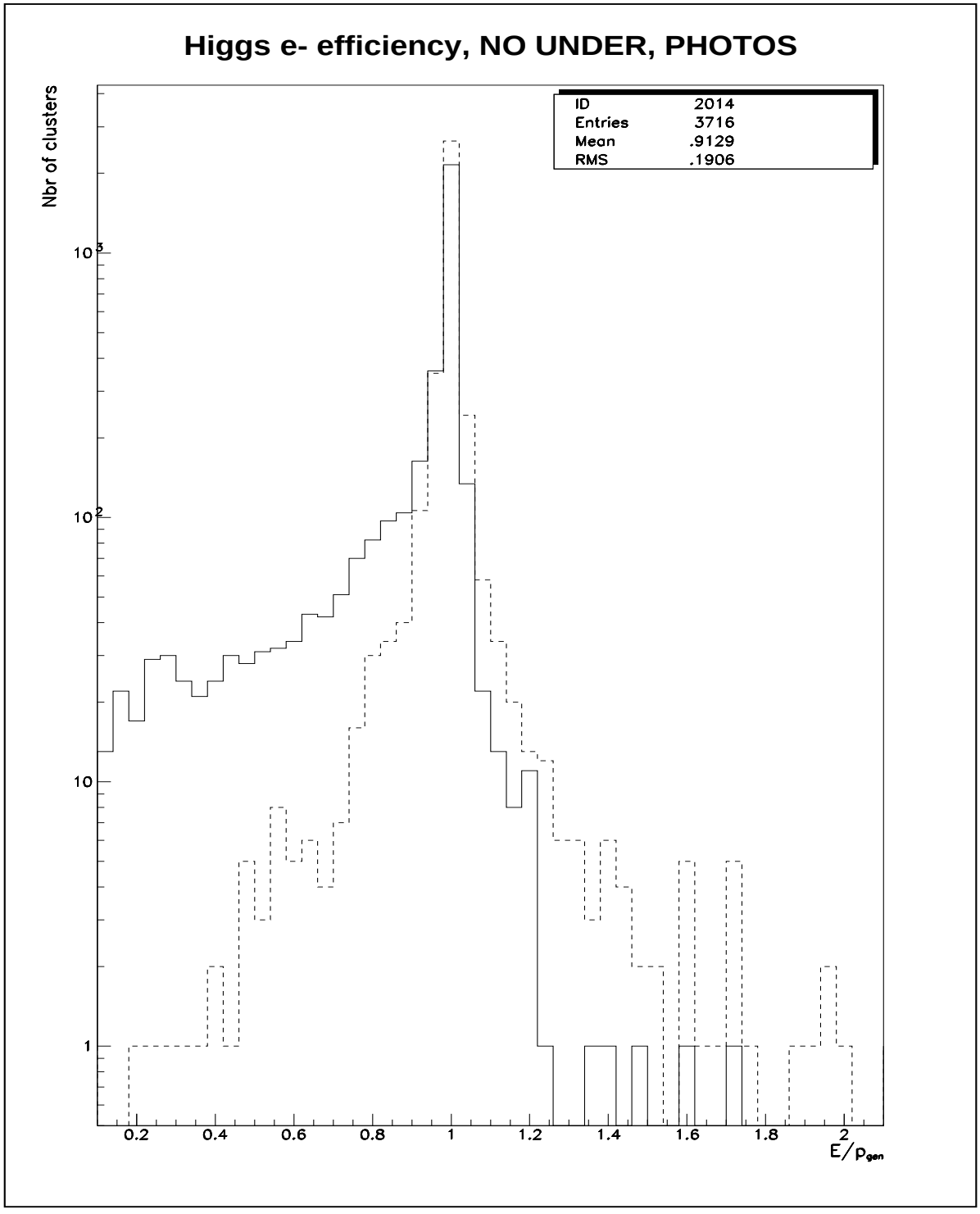

Figure 11: Same as Fig. 7 with PHOTOS internal radiation.

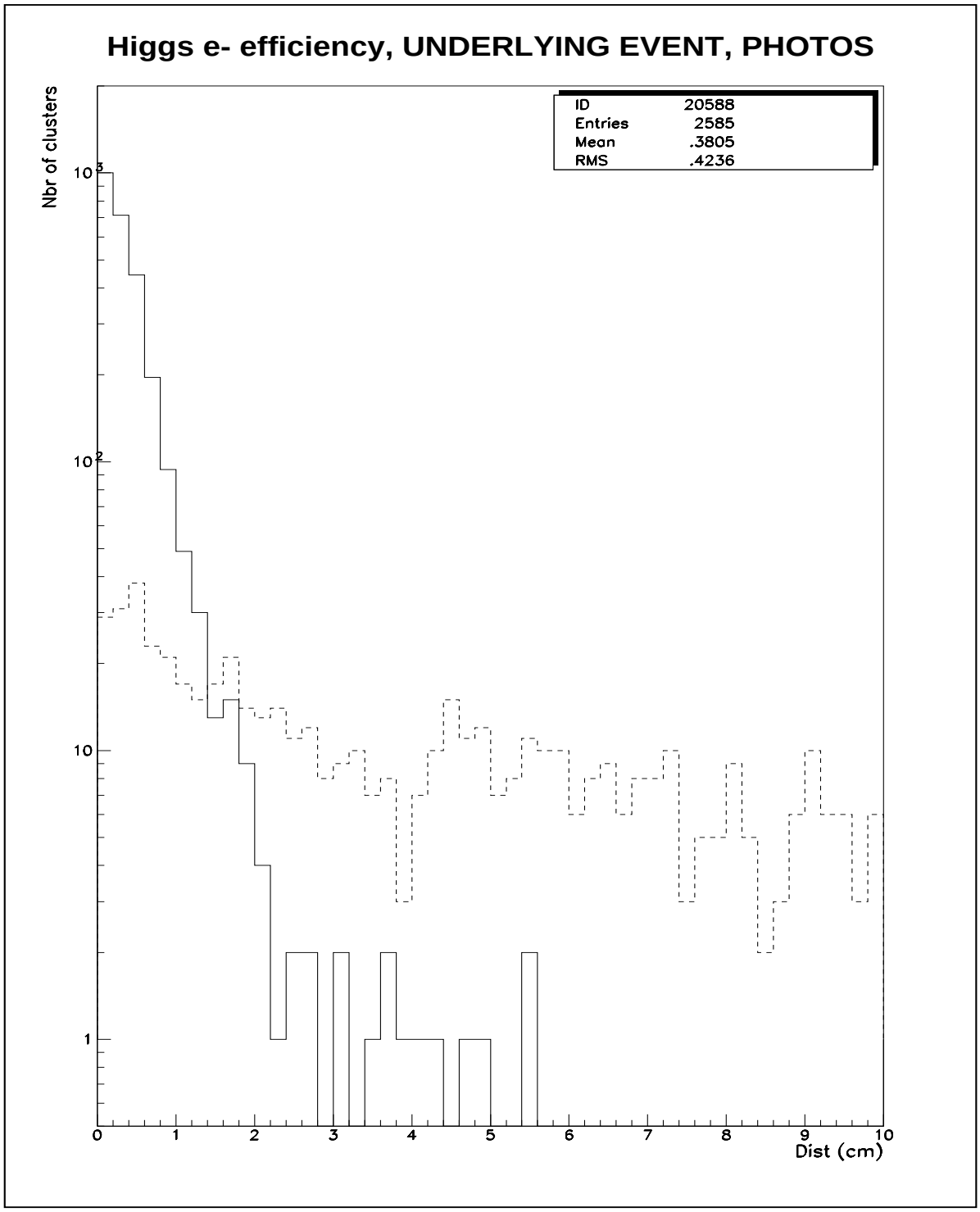

Figure 12: The distributions of distance between track and cluster for electron (solid line) and other than Higgs electron tracks (dashed line).

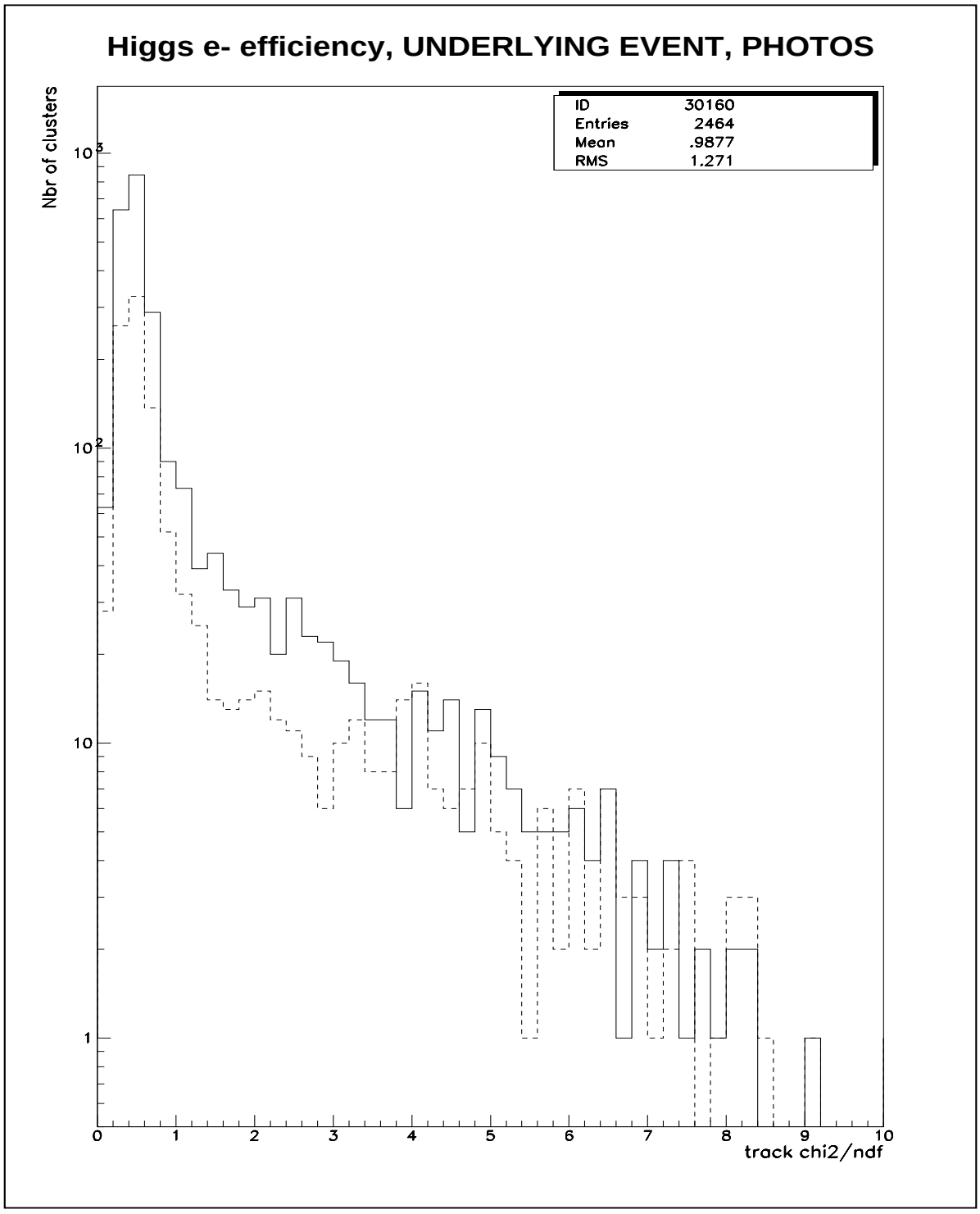

Figure 13: Tracks χ^2/ndf distributions for electrons (solid line) and other than electron tracks (dashed line).

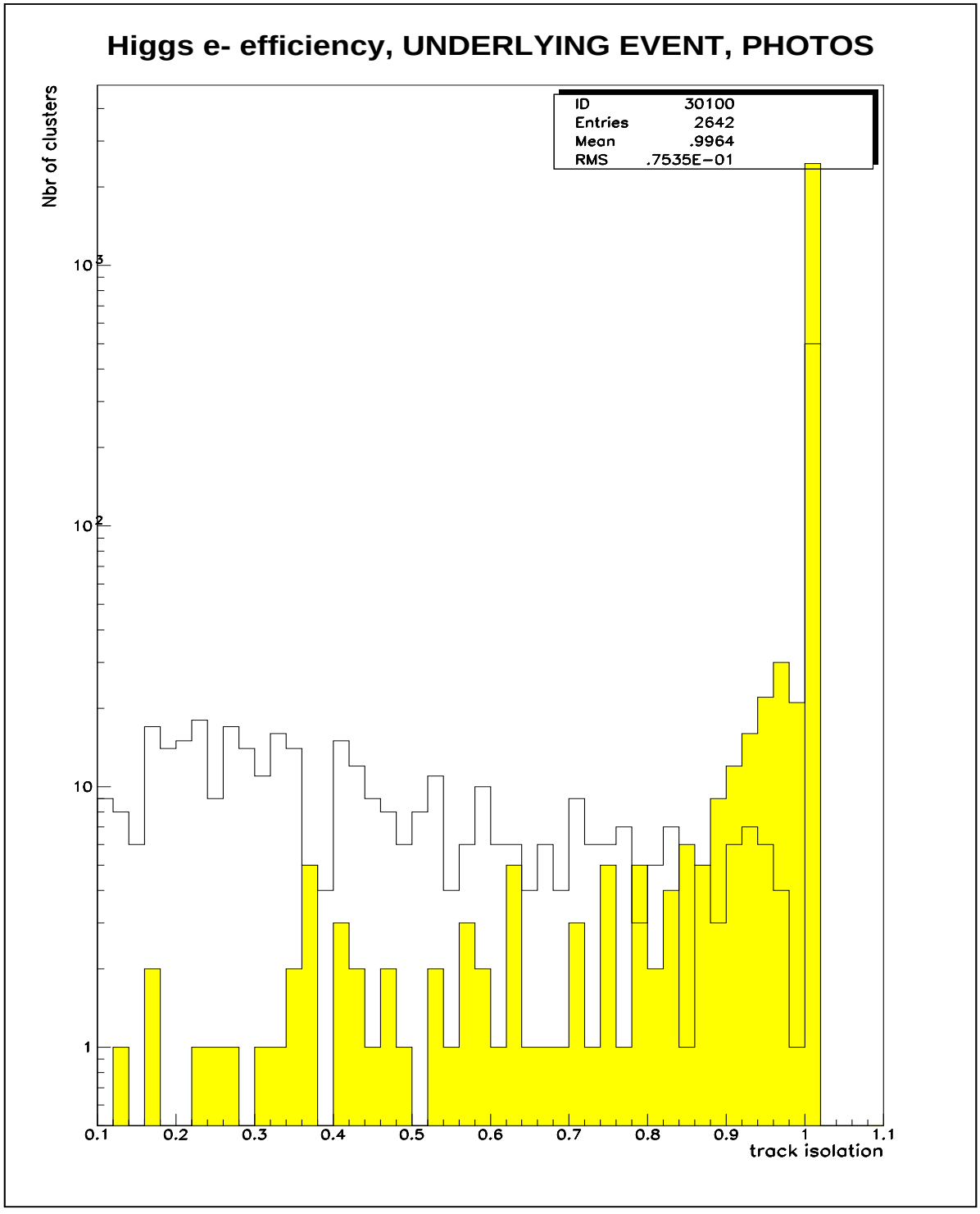

Figure 14: Isolation distributions for Higgs electrons (filled histogram) and other than Higgs electron tracks.

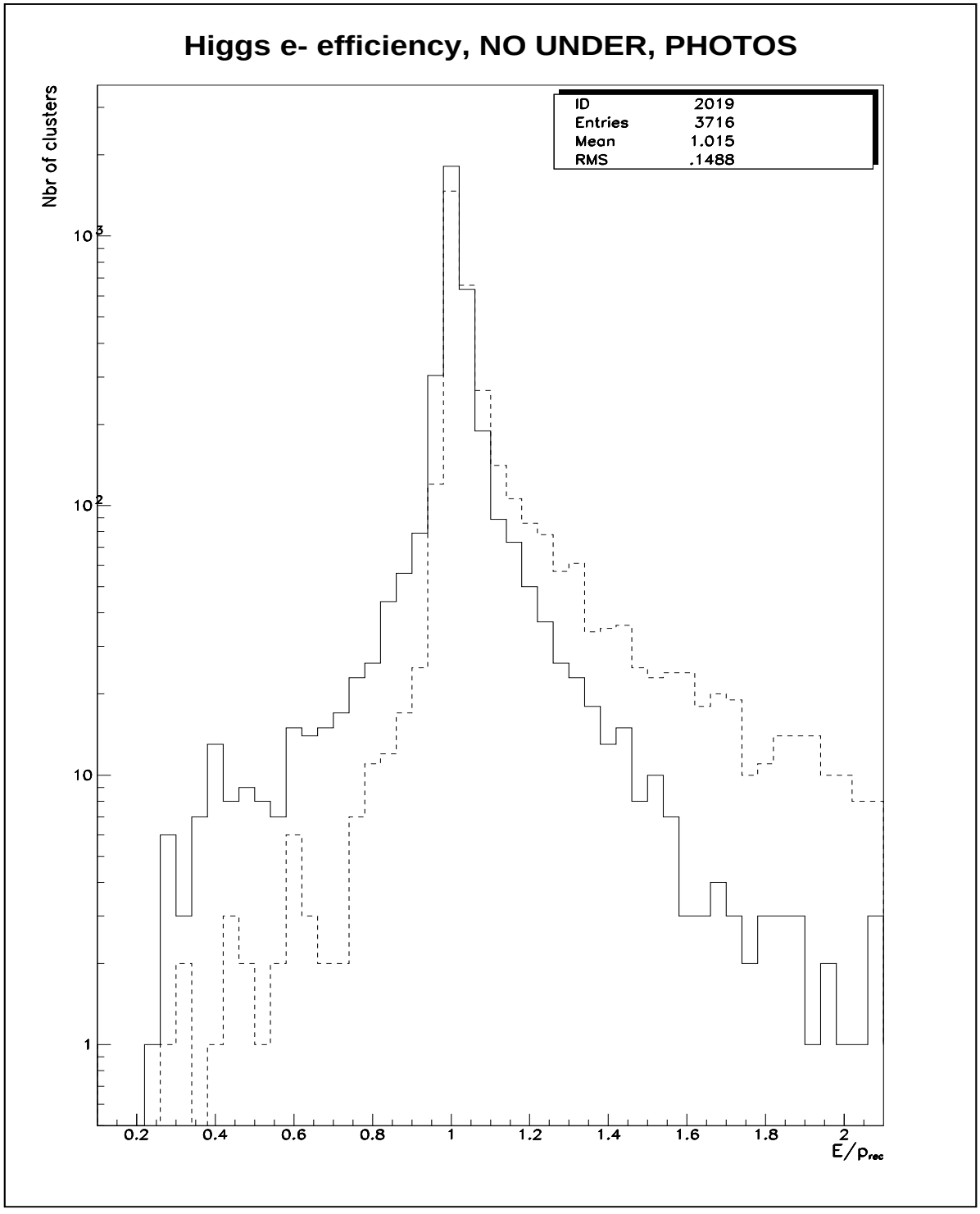

Figure 15: same as Fig. 8 with internal radiation from PHOTOS in addition of external radiation.

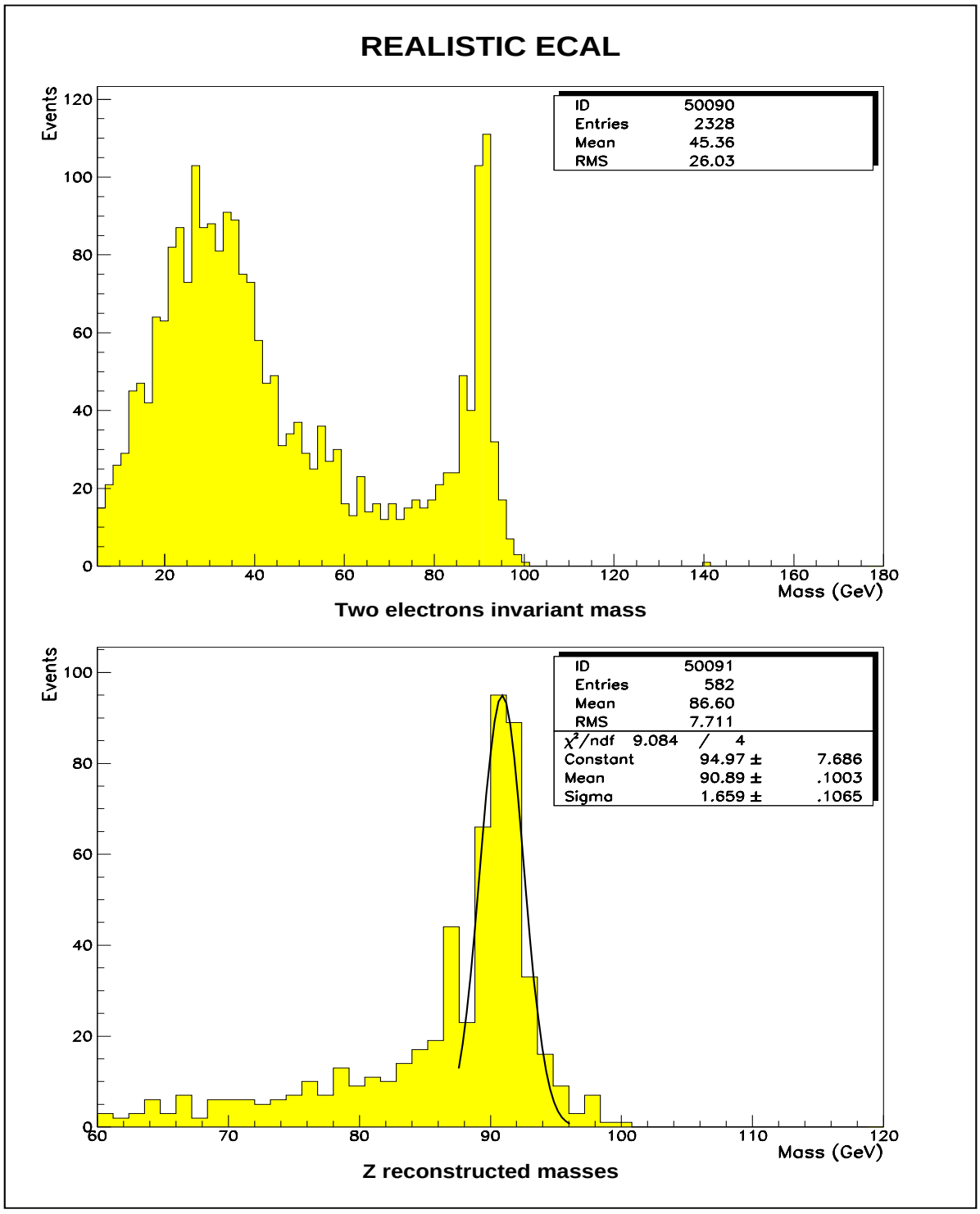

Figure 16: Z mass reconstruction with underlying event including internal radiation from PHOTOS, for the ”loose” selection and realistic ECAL.

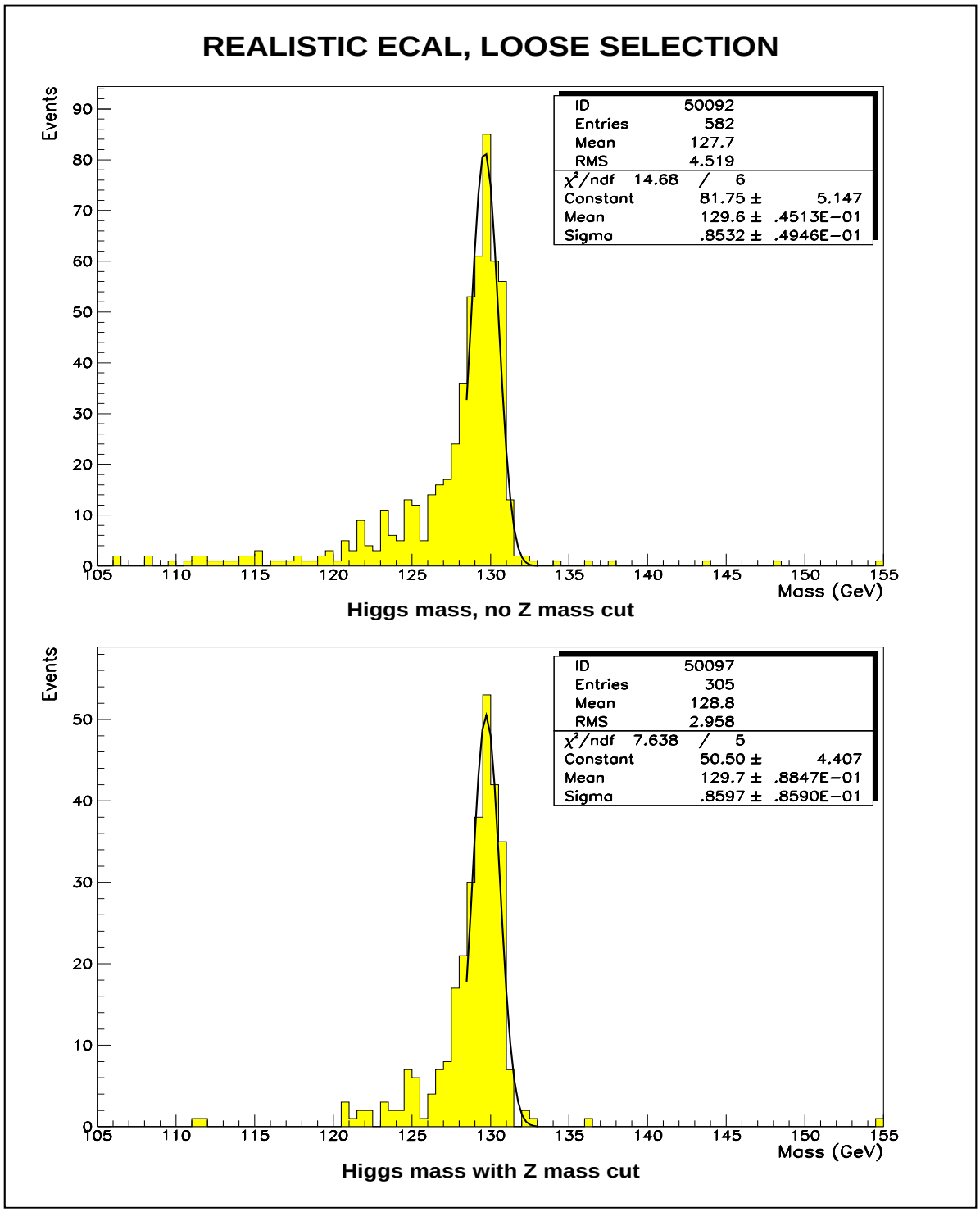

Figure 17: Higgs mass reconstruction with underlying event including internal radiation from PHOTOS, for the ”loose” selection and realistic ECAL.

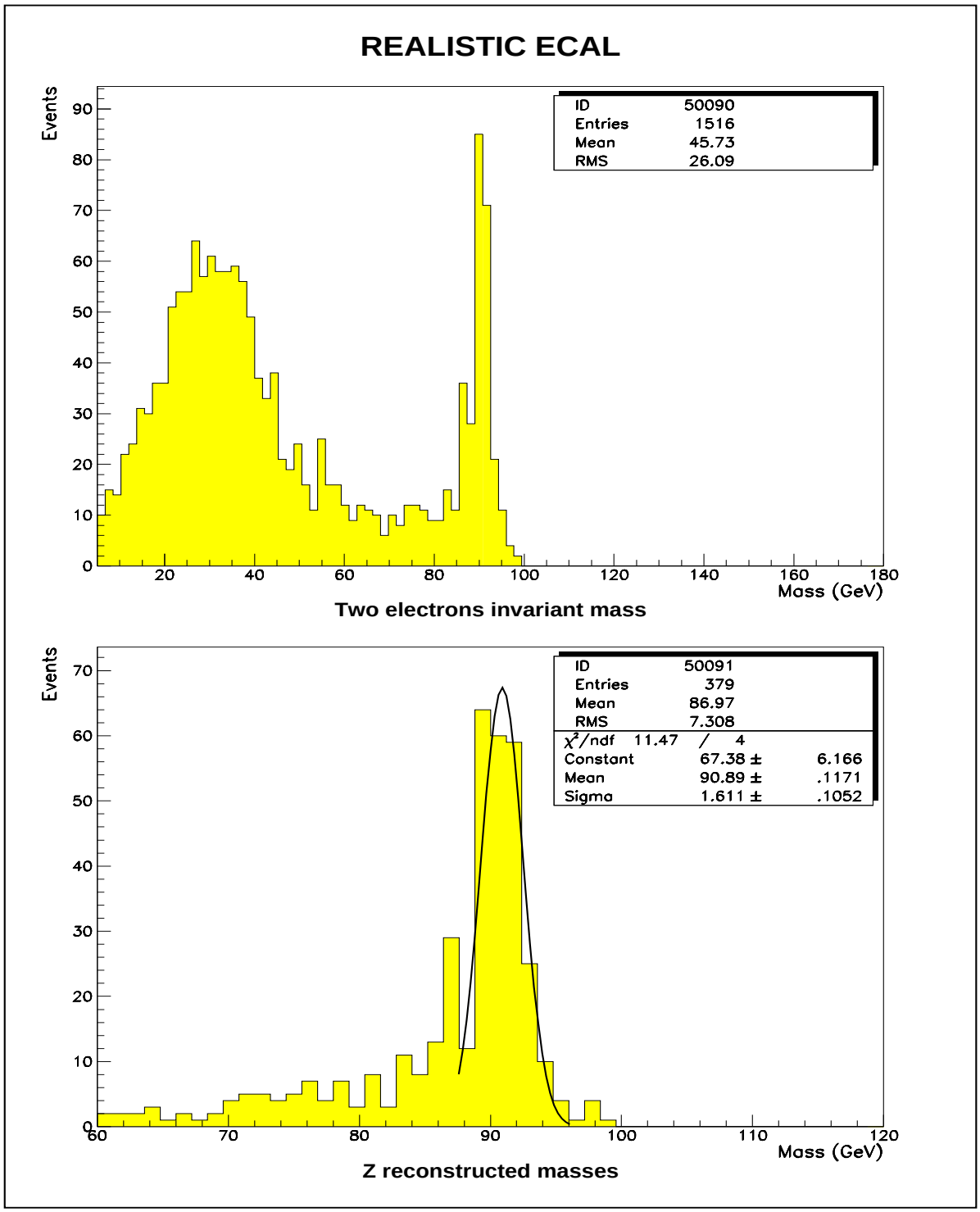

Figure 18: Z mass reconstruction with underlying event including internal radiation from PHOTOS, for the ”restricted” selection and realistic ECAL.

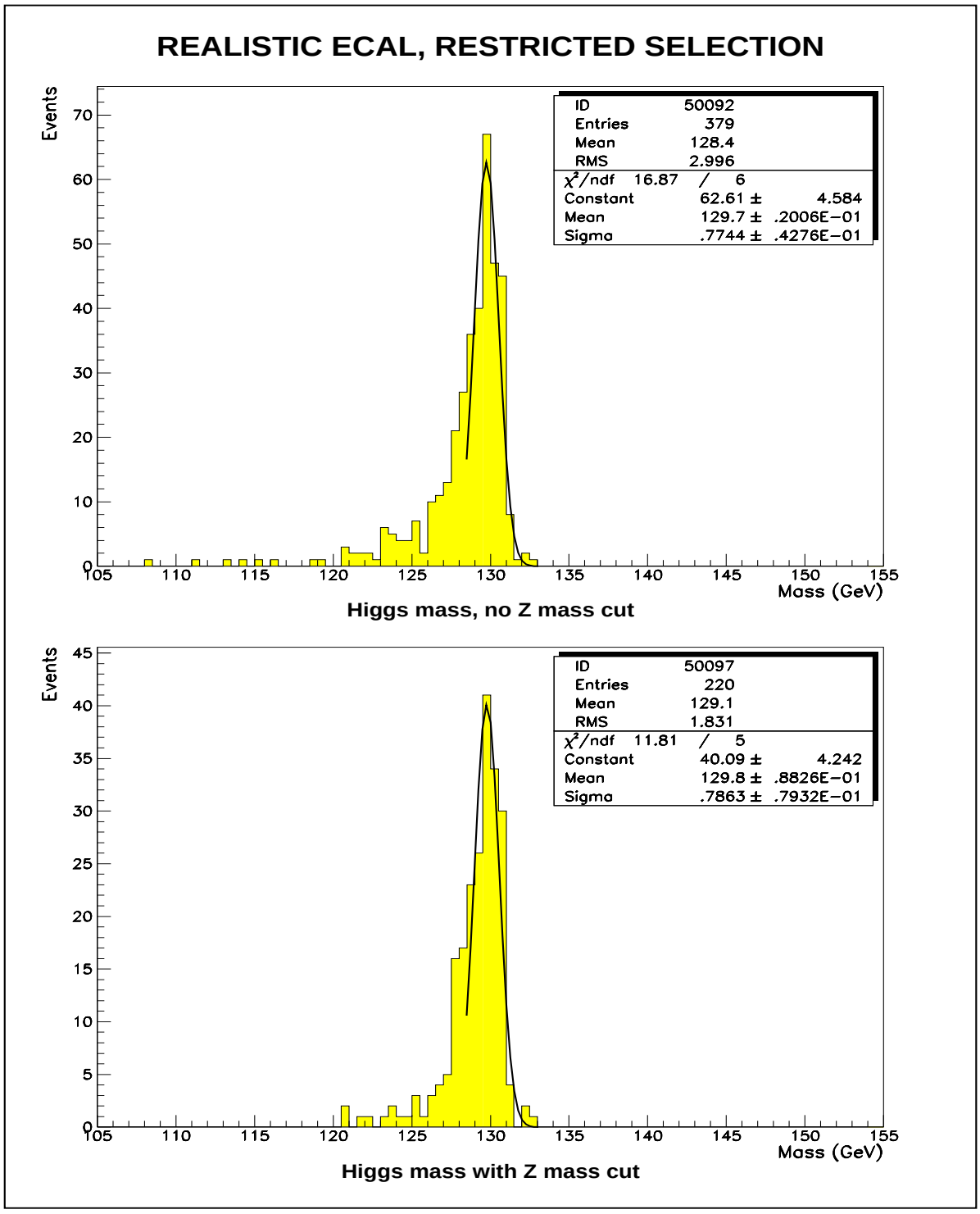

Figure 19: Higgs mass reconstruction with underlying event including internal radiation from PHOTOS, for the ”restricted” selection and realistic ECAL.

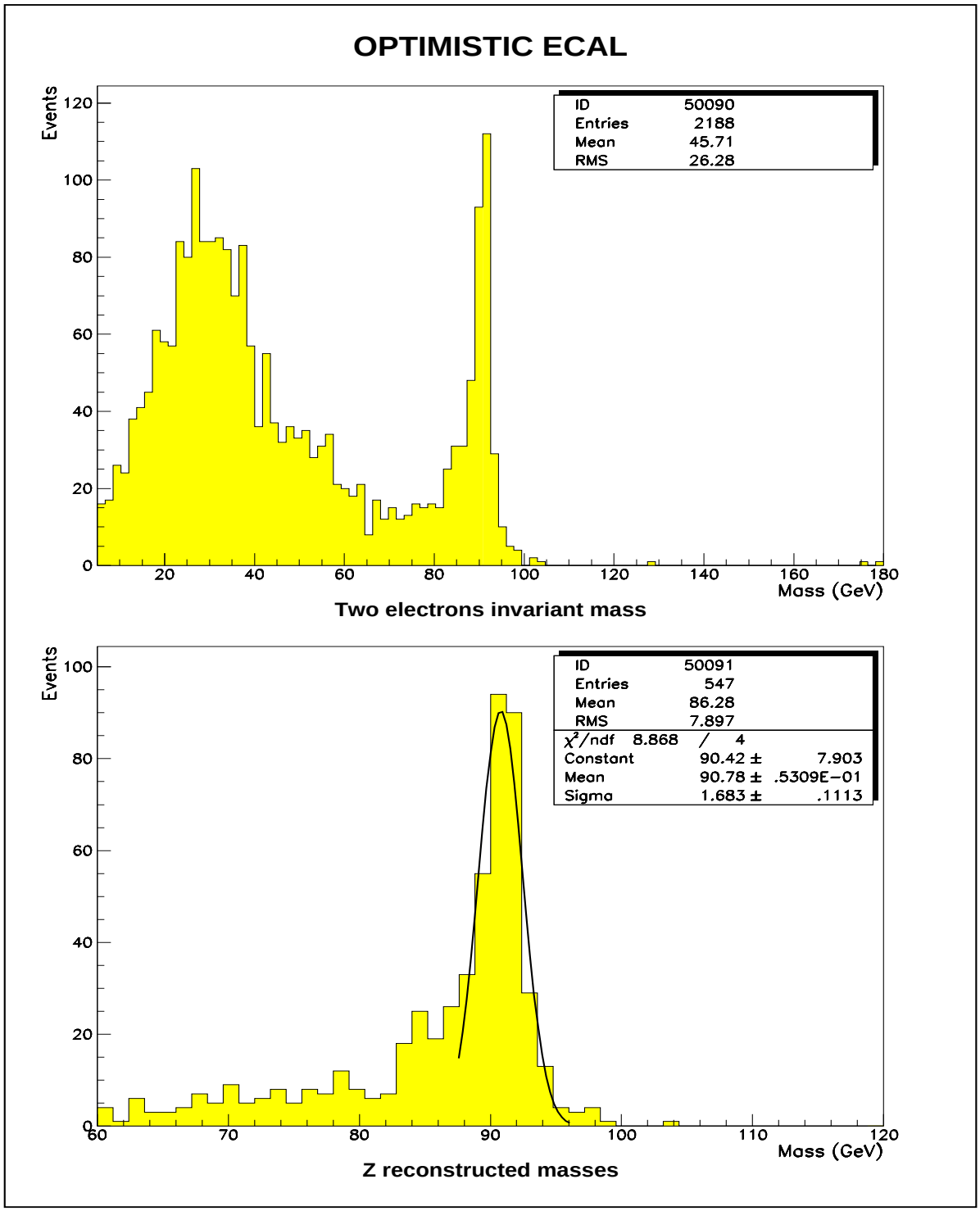

Figure 20: Z mass reconstruction with underlying event including internal radiation from PHOTOS, for the ”loose” selection and optimistic ECAL.

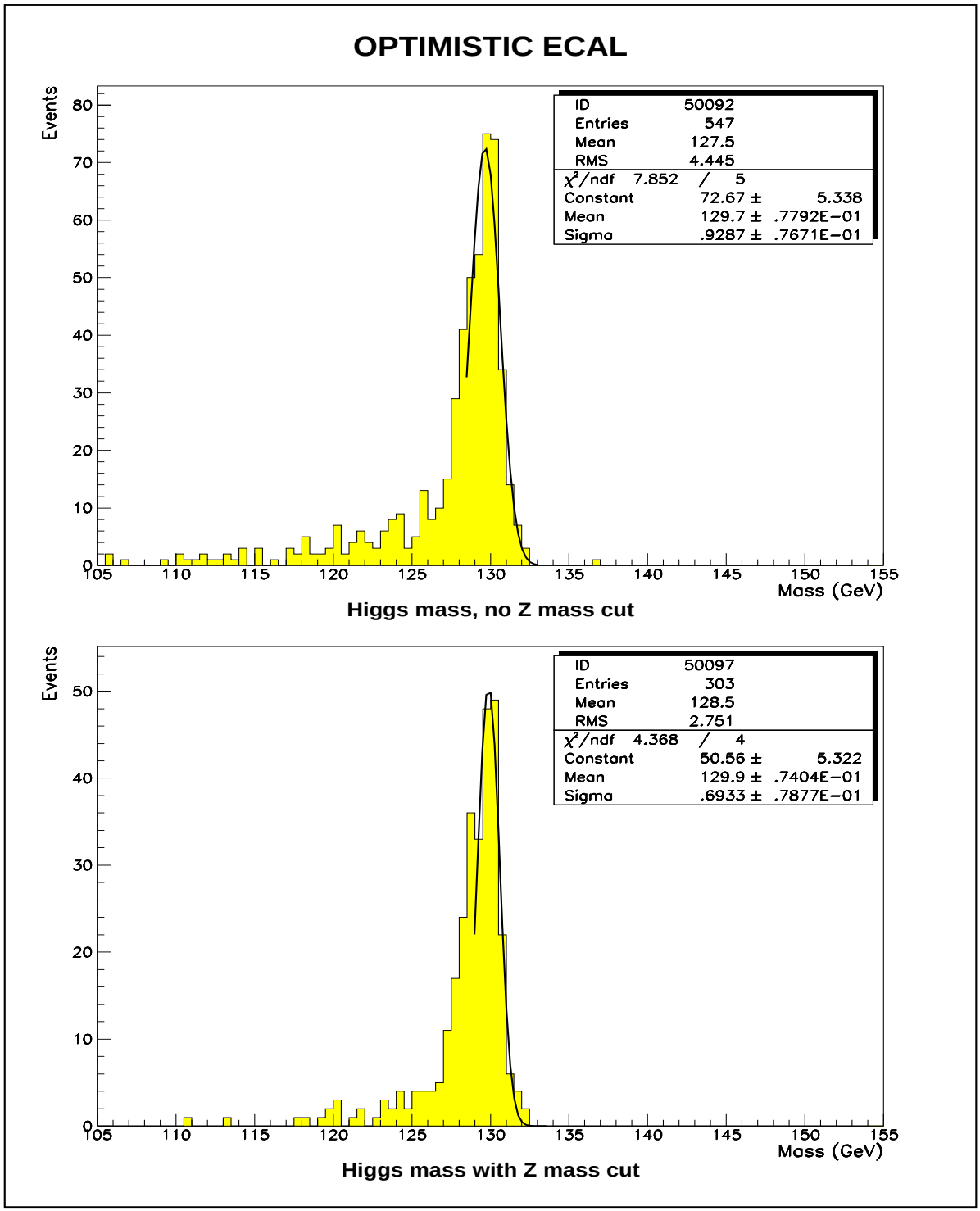

Figure 21: Higgs mass reconstruction with underlying event including internal radiation from PHOTOS, for the ”loose” selection and optimistic ECAL.

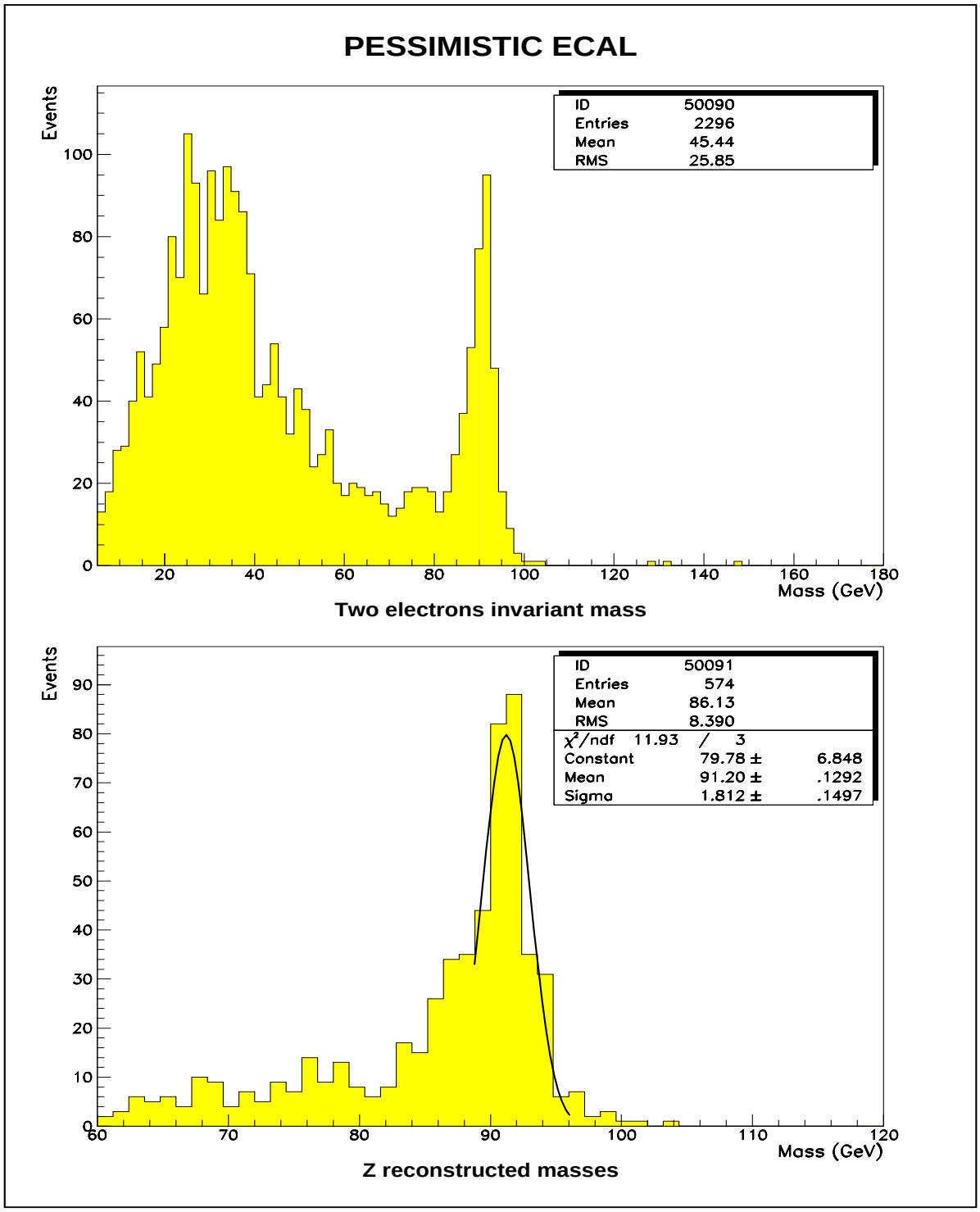

Figure 22: Z mass reconstruction with underlying event including internal radiation from PHOTOS, for the ”loose” selection and pessimistic ECAL.

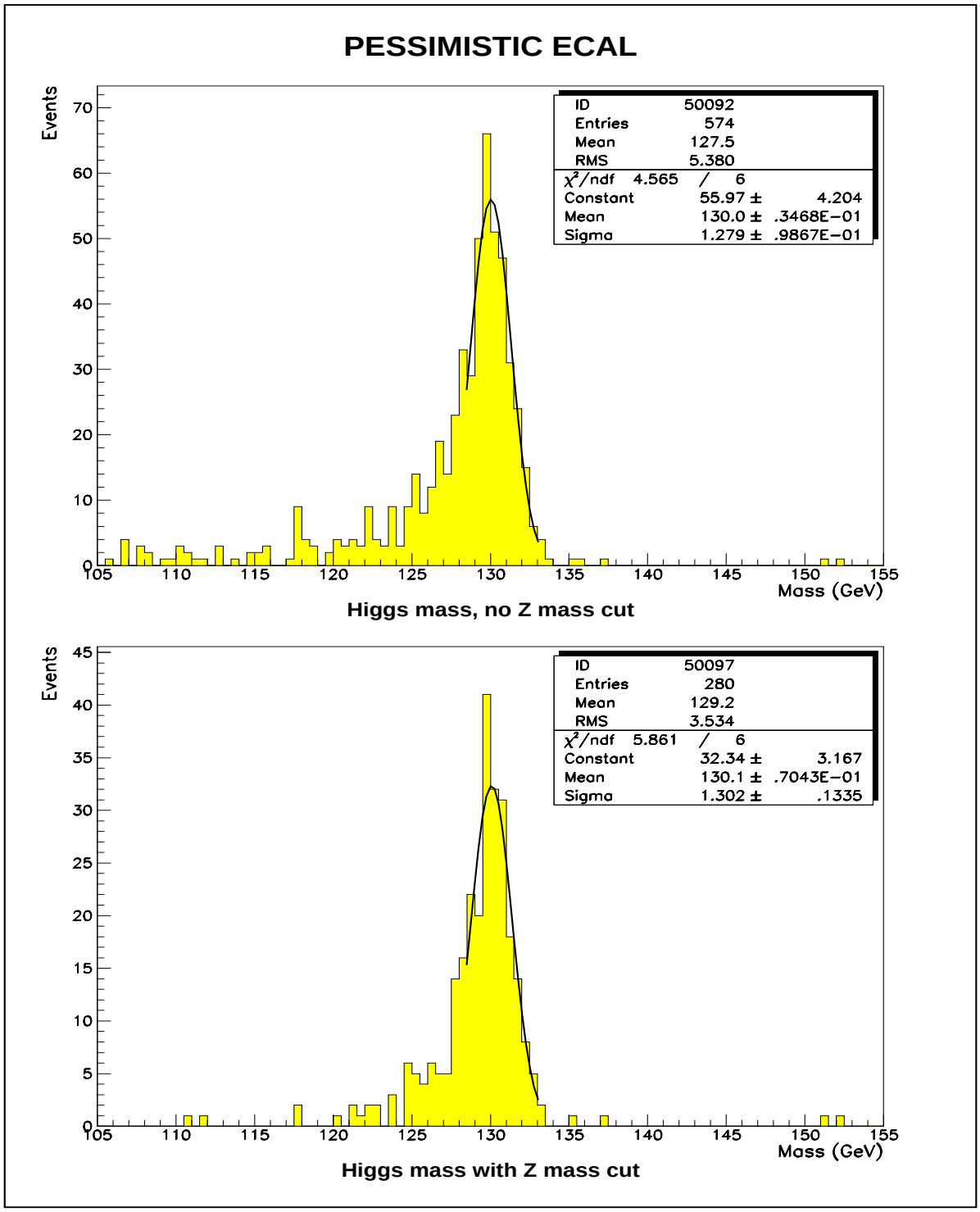

Figure 23: Higgs mass reconstruction with underlying event including internal radiation from PHOTOS, for the ”loose” selection and pessimistic ECAL.